QUANTITATIVE OBJECT RECONSTRUCTION
USING ABEL TRANSFORM TOMOGRAPHY
AND MIXED VARIABLE OPTIMIZATION

THESIS

Kevin Robert O'Reilly, Second Lieutenant, USAF

AFIT/GSS/ENC/06-1

DEPARTMENT OF THE AIR FORCE
AIR UNIVERSITY

AIR FORCE INSTITUTE OF TECHNOLOGY

Wright-Patterson Air Force Base, Ohio

APPROVED FOR PUBLIC RELEASE; DISTRIBUTION UNLIMITED

The views expressed in this thesis are those of the author and do not reflect the official policy or position of the United States Air Force, Department of Defense, or the United States Government.

AFIT/GSS/ENC/06-1

QUANTITATIVE OBJECT RECONSTRUCTION USING ABEL TRANSFORM TOMOGRAPHY AND MIXED VARIABLE OPTIMIZATION

THESIS

Presented to the Faculty

Department of Mathematics and Statistics

Graduate School of Engineering and Management

Air Force Institute of Technology

Air University

Air Education and Training Command

In Partial Fulfillment of the Requirements for the

Degree of Master of Science

Kevin Robert O'Reilly, B.S

Second Lieutenant, USAF

March, 2006

APPROVED FOR PUBLIC RELEASE; DISTRIBUTION UNLIMITED

AFIT/GSS/ENC/06-1

QUANTITATIVE OBJECT RECONSTRUCTION USING ABEL TRANSFORM TOMOGRAPHY AND MIXED VARIABLE OPTIMIZATION

Kevin Robert O'Reilly, B.S

Second Lieutenant, USAF

Approved:

Mark A. Abramson (Chairman)	date
James W. Chrissis (Member)	date

AFIT/GSS/ENC/06-1

Abstract

Researchers at the Los Alamos National Laboratory (LANL) are interested in quantitatively reconstructing an object using Abel transform x-ray tomography. Specifically, they obtain a radiograph by x-raying an object and attempt to quantitatively determine the number and types of materials and the thicknesses of each material layer. Their current methodologies either fail to provide a quantitative description of the object or are generally too slow to be useful in practice. As an alternative, the problem is modeled here as a mixed variable programming (MVP) problem, in which some variables are nonnumeric and for which no derivative information is available. The generalized pattern search (GPS) algorithm for linearly constrained MVP problems is applied to the x-ray tomography problem, by means of the NOMADm MATLAB® software package. Numerical results are provided for several test configurations of cylindrically symmetrical objects and show that, while there are difficulties to be overcome by researchers at LANL, this method is promising for solving x-ray tomography object reconstruction problems in practice.

Acknowledgements

Considering that a master's thesis cannot be accomplished without help from other, I have many people that I would like to thank for their support, guidance and encouragement during my assignment at AFIT.

Many thanks go to my advisor, Lieutenant Colonel Mark Abramson, for giving me insight that I did not have in areas I knew nothing about. I was truly fortunate to have his wealth of knowledge in the area of optimization. Throughout the year, he nudged me along the thesis route and provided vital guidance when I stalled. Additionally, my reader, Dr. James Chrissis, lent his particular expertise as a technical editor, keeping the document thorough and precise.

In addition to my committee, I wish to pay my thanks to several other individuals. I thank Dr. John Dennis for his insightful ideas and for acting as a sounding board for all of my ideas. I would also like to thank Dr. Thomas Asaki of Los Alamos National Laboratory for funding my research and providing technical background on the problem. His involvement and excitement about the problem was a huge motivating factor for me. Also, I would like to thank all of Dr. Asaki's colleagues at Los Alamos who are working in other areas of this project.

I must not leave out my companions here at AFIT. Our struggles together has made this experience endurable. Through all the joy and pain, you stuck with me and I am a better person for it.

Kevin Robert O'Reilly

Table of Contents

Page

Abstract iv

Acknowledgements v

List of Figures viii

List of Tables ix

List of Abbreviations x

I. Introduction 1-1
- 1.1 Tomography 1-1
- 1.2 Mixed-Variable Los Alamos National Lab Problem 1-2
- 1.3 Purpose of the Research 1-4
- 1.4 Overview 1-4

II. Background and Literature Review 2-1
- 2.1 Abel Inversion 2-1
  - 2.1.1 Physical Interaction 2-1
  - 2.1.2 Abel Inversion Tomography Techniques 2-3
- 2.2 Generalized Pattern Search (GPS) Methods 2-6
  - 2.2.1 Linearly Constrained GPS 2-6
  - 2.2.2 Mixed Variable GPS 2-8
  - 2.2.3 GPS extensions 2-9

III. Methodology 3-1
- 3.1 GPS for Linearly Constrained MVP Problems 3-1
  - 3.1.1 Mesh Generation 3-1
  - 3.1.2 Local Optimality 3-2
- 3.2 GPS for MVP with Linear Constraints Algorithm 3-4
  - 3.2.1 SEARCH Step 3-4
  - 3.2.2 POLL Step 3-4
  - 3.2.3 EXTENDED POLL Step 3-5
  - 3.2.4 Updating the Mesh 3-6
  - 3.2.5 Treating Linear Constraints 3-7
- 3.3 Convergence of the GPS Algorithm for MVP Problems 3-9
  - 3.3.1 Mesh Size Behavior and Limit Points 3-11

Page

3.3.2 Main Convergence Properties 3-12
3.4 GPS Algorithm Applied to the LANL Problem 3-14
3.4.1 Problem Formulation 3-14
3.4.2 Objective Function 3-15
3.4.3 Linear Constraints 3-16
3.4.4 Discrete Neighbors 3-18

IV. Numerical Results 4-1
4.1 Algorithm Implementation 4-1
4.2 Data generation 4-2
4.2.1 Experimental Conditions 4-2
4.2.2 Materials 4-4
4.2.3 Object Test Sets 4-4
4.2.4 Objective Functions 4-6
4.3 Numerical Results 4-8
4.3.1 Object Test Set 1 4-8
4.3.2 Object Test Set 2 4-9
4.3.3 Object Test Set 2 extensions 4-13

V. Conclusion 5-1
5.1 Research Conclusions 5-1
5.2 Further Research 5-2

Appendix A. Graphical Representation of Test Results A-1

Appendix B. MATLAB® Code B-1
B.1 Main Function File B-1
B.2 Parameter File B-2
B.3 Initial Iterate File B-4
B.4 Linear Constraints File B-5
B.5 Neighborhood Definition File B-6
B.6 Objective Function 1 File B-11
B.7 Objective Function 2 File B-12

Bibliography BIB-1

Vita VITA-1

List of Figures

Figure		Page
1.1	Cylindrically Spherical Object being x-rayed.	1-2
2.1	Notional Radiograph Example	2-2
3.1	Construction of the Poll and Extended Poll Sets	3-6
3.2	MVP GPS Algorithm	3-8
3.3	Directions that Conform to the Geometry of X	3-9
3.4	Algorithm for Generating Conforming Directions	3-10
3.5	Limit Points of Iterates and Extended Poll Centers.	3-12
4.1	Graphical Representation Recreation of Test Case 1f	4-10
4.2	Output from NOMADm for Test Case 1b	4-11
4.3	Graphical Representation of Test Case 2e at Different Radiograph Sizes . .	4-15

List of Tables

Table		Page
4.1	Possible Materials.	4-5
4.2	Adjacency Matrix.	4-5
4.3	Test Set 1 Object Configuration.	4-6
4.4	Test Set 2 Object Configuration.	4-7
4.5	Object Test Set 1, Single Attenuation Value Objective Function, Summation Radiographs.	4-9
4.6	Object Test Set 2, Single Attenuation Value Objective Function, Summation Radiographs.	4-12
4.7	Object Test Set 2, Vector Attenuation Value Objective Function, MCNP No Scatter Radiographs.	4-12
4.8	Object Test Set 2, Vector Attenuation Value Objective Function, MCNP Scattering Radiographs.	4-14
4.9	Test Case 2e, Vector Attenuation Value Objective Function, MCNP No Scattering Radiographs at Different Sizes or Radiographs Used.	4-14

List of Abbreviations

Abbreviation		Page
LANL	Los Alamos National Laboratory	1-2
MVP	mixed variable programming	1-4
GPS	generalized pattern search	1-4
KeV	kilo-electron-volts	2-1
MeV	mega-electron-volts	2-3
KKT	Karush-Kuhn-Tucker	2-7
MADS	mesh adaptive direct search	2-10

QUANTITATIVE OBJECT RECONSTRUCTION USING ABEL TRANSFORM TOMOGRAPHY AND MIXED VARIABLE OPTIMIZATION

I. Introduction

1.1 Tomography

Tomography refers to the "cross-sectional imaging of an object from either transmission or reflection of data collected by illuminating the object from many different directions" [34, 5]. The majority of the research in computerized tomographic techniques has been focused on diagnostic medicine which allows doctors to quickly and safely view a patient's internal organs. Originally based on the x-ray attenuation coefficient (how much x-ray intensity is decreased) of organic tissues, medical imaging computer tomography, with the help of modern computers, has branched into different types of imaging, such as using radioisotopes, ultrasound, and magnetic resonance.

In addition to medical imaging, tomography has been applied to qualitative object imaging in areas outside of medicine, such as mapping of underground resources, nondestructive testing of engineered parts such as rocket engines, brightness distribution determination of a celestial sphere, and three-dimensional imaging using an electron microscope [34, 1-2].

Although the inversion of a cylindrically symmetric object was solved analytically by Abel [2] in 1826, resulting in Abel inversion techniques, there did not exist a way to image the interior an object until the discovery of the powerful uses of x-rays. In 1917, Radon discovered a way to mathematically reconstruct any function from its projections, but his methods produce inexact reconstructions that are only useful in qualitative analysis, such as medical imaging. With the development of modern computers, Houndsfield invented in 1972 the first x-ray computed tomographic scanner, which could recreate an object's image from its x-ray projections [34, 1-2].

1.2 Mixed-Variable Los Alamos National Lab Problem

Researchers at the Los Alamos National Laboratory (LANL) are interested in fast (minutes) quantitative object reconstructions from x-ray radiographs. In particular, they wish to make use of the Abel transform to determine the composition of a cylindrically symmetrical object made of concentric material layers. In order to do so, the material type and thickness of each concentric layer must be identified. Figure 1.1 shows pictorially the lateral section of a cylindrically symmetric object composed of four material layers. The shading represents different materials, while the concentric circles denote the outer edge of each material layer. The dashed lines represent the x-rays, while the horizontal line at the bottom of the picture represents the detector.

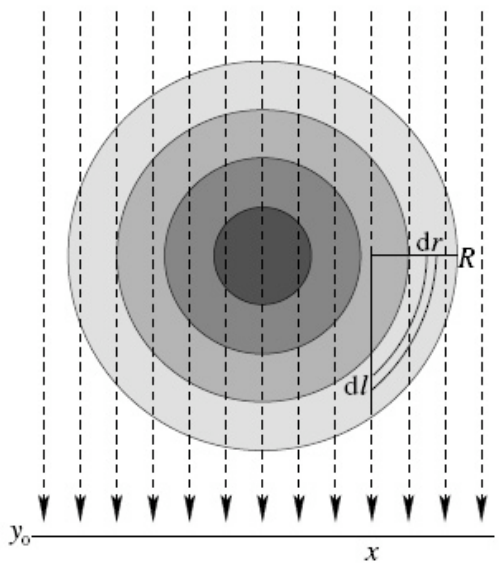

Figure 1.1: Cylindrically Spherical Object being x-rayed.

Current work at LANL includes computation of Abel transform inverses, but this approach has some inherent difficulties. As an alternative, researchers at LANL have turned to mathematical

optimization techniques in an attempt to minimize the error between x-ray radiograph data and likely object configurations.

Many engineering design problems involve minimizing or maximizing a measure of system performance by changing values of the design variables subject to some set of design constraints. For example, a structural engineer may need to find the minimum width of a beam subject to a maximum expected load. Many optimization problems can be solved numerically, using a gradient or Newton-based algorithm, but these will not work for the LANL problem due to the lack of derivative information.

Some problems have design variables that can only take on integer values. For example, suppose the structural engineer can only obtain steel beams in 2, 3, 4, or 5 foot widths from a foundry. This class of problems can be treated by temporarily relaxing the integrality of these variables during portions of the algorithm, but which reinforce this restriction in the final solution.

Even more challenging are problems with discrete variables that can only be set to certain values, and for which temporary relaxation makes no physical sense. These variables are *categorical*, meaning that their values must always be chosen for a pre-defined list and may even be nonnumeric. For example, the structural engineer may be able to choose between multiple types of metals for the beam. Categorical design variables with nonnumeric values can be assigned discrete values, based on index numbers in the list, such as $1 =$ iron, $2 =$ steel, $3 =$ titanium, etc. However, it is not possible to perform meaningful calculations on the assigned values. For example, material 2 may not be twice as strong as material 1. Additionally, solution approaches that temporarily relax the integer restrictions break down in the face of categorical variables. For example, in the case described, a value of 1.5 has no physical meaning in terms of the materials. Parametric studies are often conducted with categorical variables in which specific fixed values of the categoric variables are compared against each other. Although effective for a small number of design variables, this method is impractical for problems with even a moderate number of design variables, as in the LANL problem. Finally, various meta-heuristics can also be applied to improve the design, but they do not typically possess convergence properties that could even guarantee local optimality.

Problems with continuous and categorical variables are known as *mixed variable programming* (MVP) problems. The LANL problem belongs to this class of problems. In order to describe the composition of the cylindrically symmetrical object in the LANL problem, the design variable, $x = (x^c, x^d)$, is partitioned into two parts. The first part contains the layer edge location information as a continuous variable, $x^c \in \mathbb{R}^{n^c}$, while the second part contains the material type as a discrete variable, $x^d \in Z^{n^d}$. This partitioning of the solution leads to an MVP of the following form

$$\min_{x \in X} \quad f(x) \tag{1.1}$$

where $f : X \to \mathbb{R}$ and the domain $X = X^c \times X^d$ is also partitioned, with $X^c = \{x \in X : l \leq Ax^c \leq u\} \subseteq \mathbb{R}^{n^c}$ and $X^d \subseteq \mathbb{Z}^{n^d}$. The material type is selected from a predefined material library, while the thicknesses of the materials, as determined from the material edge locations, are subject to linear constraints with $A \subseteq \mathbb{Q}^{m \times n}$ and $l, u \in (\mathbb{R} \cup \{\infty\})^m$. More detail is provided in Chapter III.

1.3 Purpose of the Research

Algorithms for solving MVP problems are scarce. However, a class of algorithms, known as *generalized pattern search* (GPS) methods, has developed over the past ten years that can solve MVP problems with linear constraints. The purpose of the research in this thesis is to apply a MVP GPS algorithm to the LANL problem, and to establish a methodology for determining the composition of cylindrically symmetrical objects made of concentric material layers from x-ray radiograph data.

1.4 Overview

The remainder of this document is laid out as follows. Chapter II contains a review of appropriate literature covering the physics of x-ray tomography and approaches that have been taken to overcome difficulties inherent in Abel inversion. Additionally, the literature containing the development GPS algorithms is reviewed. Chapter III describes the LANL x-ray tomography problem

in detail, as well as the GPS algorithm for MVP problems with linear constraints. Chapter IV describes the numerical implementation used to solve the object reconstruction problem, followed by numerical results on test problems provided by LANL, as well as an analysis of the effectiveness of the approach. Finally, Chapter V discusses conclusions and recommendations for future research.

II. Background and Literature Review

In order to appropriately apply the generalized pattern search (GPS) algorithm with linear constraints to the x-ray tomography problem, it is necessary to identify the physical interactions inherent in x-ray radiography and how they cause difficulties in object reconstruction tomography. Literature on previous work utilizing Abel inversion techniques as a way to preform object reconstruction is also reviewed. Additionally, through the review of GPS, the evolution of the GPS algorithm from its initial development used to solve unconstrained nonlinear programs to its extension to MVP problem is traced.

2.1 Abel Inversion

2.1.1 Physical Interaction. Although the Radon transform is generally used in x-ray tomography, the Radon transform reduces to the Abel transform, which exactly reconstructs a cylindrically symmetrical object from a single x-ray radiograph. However, difficulties in utilizing the Abel transform arise for several reasons that include the physics of x-ray radiography, as well as properties of the Abel transform itself, as it applies to this problem.

X-rays are electromagnetic waves propagating through space, forming beams of photons. When these beams interact with electrons or protons within the atoms of a material, they accelerate in different directions, due to one of three types of photon scattering. Both [34, 114] and [13] address the difficulties invoked by the physics of x-ray scattering on the recreation of an object, although discussion in [34, 114] is limited to problems commonly encountered in medical diagnostic imaging (from 20 to 150 kilo-electron-volts (KeV)).

At the simplest level, an x-ray radiograph can be thought of as a projection of an object onto a radiography formed by the attenuation or disturbance of the x-ray beams as they pass through a certain amount of material between the x-ray source and the detector. If several radiographs are taken from different viewing directions, it may be possible to recreate the shape of the original object. Figure 2.1 [34, 2] shows how this could be accomplished. The objects being x-rayed are

the two circles in the center of the figure. The diagonal planes on the left and right side of the image represent the radiographs with their associated shadows. The two objects are x-rayed from two different viewing directions, once from the lower left and once of the lower right. By knowing the viewing angles and examining the shadows on both radiographs, it is possible to determine that the original objects consisted of two circles, one being smaller than the other.

This example is a highly simplified case because x-rays interact with charged particles (protons and electrons) in matter in complex processes that are a combination of scattering, attenuation, and energy changes that are all material and energy-level dependent, making the recreation difficult [13].

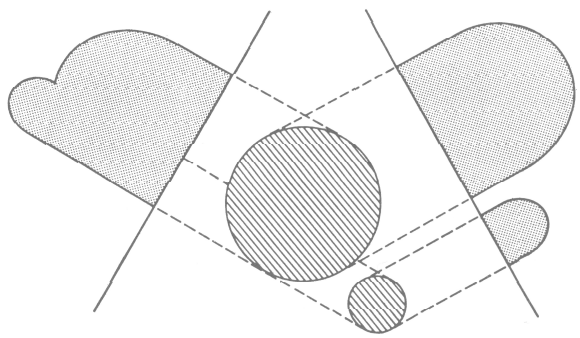

Figure 2.1: Notional Radiograph Example

There are three types of scattering. The first type, known as the *photoelectric effect* [13] occurs when an x-ray photon interacts with a tightly bound inner electron. As a result, all of the x-ray photon's energy is absorbed into the movement of the electron, causing it to temporarily increase its energy level or completely leave the atom (as is the case with metals). When the electron returns to its original energy state, it releases its gained energy in the form of a photon, emitted in a random direction. As a result, the newly created photon is most likely traveling in a different direction from that of the incident angle of the x-ray photon.

The second type of scattering is referred to as *Compton scattering* [13]. In this case, the x-ray photon interacts with a loosely bound outer electron and scatters off at an angle, while imparting some of its energy to the electron. Unlike the photoelectric effect, there is a strong angular correlation between the incoming angle and the scattered angle. As a result, the reduced energy photon is much more likely to be traveling in, or close to, its original path, parallel to the other x-ray photons, than to bounce back in the direction from which it came from.

The final type of scattering, called *pair production*, occurs with photons with energies higher than 1.022 mega-electron-volts (MeV). When high energy photons interact with an atom, they temporarily produce an electron/positron pair that immediately destroy each other, producing two photons of 0.511 MeV traveling in random but opposite directions. If the energy of the original photon is higher than 1.022 MeV, the remaining energy would stay with the original photon [13].

As previously stated, these scattering processes are energy dependent. For medical imaging as well as field deployed x-ray radiography devices, it is impractical to use x-rays that contain mono-energetic (one energy level) photons because high intensities and high energies are difficult to obtain from mono-energetic sources and are generally limited to laboratory applications. As a result, polychromatic (multi-energetic) x-ray sources, which produce x-rays of varying photon levels, are used because they are inexpensive and portable compared to monochromatic sources. However, polychromatic sources only exacerbate the scattering issues addressed above because x-ray photons of different energy levels scatter differently.

Another physical phenomenon, known as *beam hardening*, makes x-ray tomography difficult when using a polychromatic source. It occurs because the linear attenuation coefficient (the amount the x-ray's intensity is reduced) is energy dependent. As a result, the beam's spectral content (the distribution of the x-ray beam's energy) is different at the detector than at the source [34, 118].

2.1.2 Abel Inversion Tomography Techniques. Despite the difficulties identified in Section 2.1.1, researchers at LANL believe that the Abel transform is useful for describing the tomographic measurement operator. In simplest terms, this operator is a linear transform P that maps

the object's properties μ to the measured quantities d, obtained from the radiograph.

$$P\mu = d \tag{2.1}$$

Ideally, (2.1) could be solved simply by taking the inverse P^{-1} of the linear transform. However, in x-ray tomography problems for cylindrically symmetric objects, such as in [14], detectors measure photon intensity, and in order to determine the object's density properties, intensity data must be converted to the attenuation coefficient. This is accomplished through the use of the inverse Abel transform. In [14], the authors consider a one-dimensional recreation of the object from a single radiograph with a single property description, $\mu(r)$, where r is the radial distance from the center of the object. Neglecting the physical interactions of scattering, the continuous inverse Abel transform for this case may be expressed as

$$\mu(r) = -\frac{1}{\pi r}\frac{d}{dr}\int_r^\infty \frac{xd(x)}{\sqrt{x^2 - r^2}}, \tag{2.2}$$

where the attenuation coefficient μ is a line integral relative to the intensity d and x is the distance on the radiograph.

However, direct inversion of the Abel transform is difficult because there is a singularity in (2.2) at the lower limit of the integral. In order to address this difficulty, Asaki et al. [14] suggest using the Abel transform,

$$d(x) = 2\int_{|x|}^\infty \frac{r\mu(r)}{\sqrt{r^2 - x^2}}dr, \tag{2.3}$$

and not its inverse. The Abel transform is then discretized and formulated as a non-sparse matrix $P \in \mathbb{R}^{m\times n}$ with $\mu \in \mathbb{R}^n$ and $d \in \mathbb{R}^m$.

Other methods of performing indirect Abel inversion include fitting simple polynomial functions (up to twelfth-order) to the data, or performing least-squares curve fitting methods and then

directly inverting [24]. In [49] the data is filtered using its Fourier Transform, while in [46] the Abel transform is fit to the data by expanding the inverse with respect to a chosen basis.

Although the formulation of P as a matrix avoids the integral singularity in (2.2), discretization produces poor results for several reasons [14]. First (2.3) is highly simplified and does not take into account the physical interactions of scattering and polychromatic effects. Second, if $m < n$, P is singular and thus cannot be inverted. Third, even when $n \approx m$ and P^{-1} exists, P becomes ill-conditioned, meaning that small changes in d will lead to large deviations in μ, resulting in noise amplification.

To overcome these difficulties, it is necessary to smooth or *regularize* the Abel transform before it can be applied for quantitative evaluation. Asaki [12] suggest various regularization techniques, which attempt to suppress noise growth in the inversion process and preserve data discontinuities that help locate material edges. They use these techniques to regularize the discrete Abel transform to minimize the function

$$\min_{\mu} F(\mu) = \min_{\mu}\{\|P\mu - d\| + \alpha R(\mu)\} \tag{2.4}$$

where $\|.\|$ is a data fidelity norm that measures how well the object matches the data, α is the regularization parameter chosen to estimate the variance of the data, and R is the regularization function chosen.

The solution of (2.4) depends on several factors. First, the correct data fidelity norm must be chosen. Second, the minimization will depend on both $R(\mu)$ and α. In [14], F was minimized many times at different values of α. This final solution is provided by the α for which the chosen data fidelity norm produces the known or estimated variance of the data. In [15], a regularization function is extended and applied to a cylindrically symmetrical three-dimensional object represented in cylindrical coordinates.

Although these regularizations have proven successful in suppressing noise, they are unable to incorporate any significant prior knowledge about the object. Additionally, there is no way to

quantitatively determine the object's material composition or even the number of layers in the object. As a result of these difficulties, LANL researchers are turning to optimization methods that avoid relying on regularization functions in order to find a quantitative solution to object reconstruction that can take advantage of all prior knowledge of the object. In the next chapter, the mixed variable pattern search algorithm is presented as a suitable approach to solving x-ray Abel transform tomography object reconstruction problems.

2.2 Generalized Pattern Search (GPS) Methods

2.2.1 Linearly Constrained GPS. Generalized pattern search falls into the category of direct search methods, which do not compute or approximate derivatives of the objective function f. In a 1997 paper, Torczon [51] presents the class of GPS methods for solving unconstrained minimization problems as a generalization of some other well-known methods, such as coordinate search with fixed step sizes, evolutionary operation using factorial design [21], Hooke and Jeeves' original direct search algorithm [33], and the multidirectional search algorithm [27]. In doing so, she included a unifying convergence theory that does not require derivative information or a sufficient decrease conditions.

At each iteration, the objective function f is evaluated at points lying on a mesh or lattice. The mesh is defined as the set of all nonnegative integer combinations of vectors that form a positive spanning set (see Definition 2.2.1). During each iteration, the mesh points lying adjacent to the current iterate are evaluated. If improvement is found, the point is accepted and the mesh is either retained or coarsened; otherwise, the mesh is refined by decreasing the mesh size. By limiting the search to points on the mesh, Torczon [51] was able to show that if all iterates lie in a compact set and the function f is continuously differentiable, then the mesh size becomes arbitrarily small. As a result, there exists a subsequence of iterates that converges to a point x^* that satisfies the first-order necessary condition, $\nabla f(x^*) = 0$. More detail is given in Chapter III.

Lewis and Torczon [40] improved the efficiency of the algorithm in [51] by applying the theory of a positive linear dependence [25]. In doing so, they were able to lower the worst case

cost of an iteration from $2n$ to $n+1$ function evaluations while maintaining existing convergence properties.

The following key definition and theorem come from [25]:

Definition 2.2.1 *A finite set of vectors $W = \{w_i\}_{i=1}^r$ forms a* positive spanning set *for $\mathbb{R}^n$, if every $v \in \mathbb{R}^n$ can be expressed as $v = \sum \alpha_i w_i$ for some α_i, $i = 1, 2, \ldots, r$. The set of vectors W is said to* positively span $\mathbb{R}^n$. *The set W is said to be a* positive basis *for $\mathbb{R}^n$ if no proper subset of W positively spans $\mathbb{R}^n$.*

Theorem 2.2.2 *A set D positively spans $\mathbb{R}^n$ if and only if, for all nonzero $v \in \mathbb{R}^n$, $v^T d > 0$ for some $d \in D$.*

Theorem 2.2.2 ensures that if $\nabla f(x)$ exists at x and is nonzero, then (by choosing $v = -\nabla f(x)$) there exists a $d \in D$, such that $\nabla f(x)^T d < 0$. Thus, at least one $d \in D$ is a direction of descent. In pattern search, two very common choices for a positive basis include the columns of $D = [I, -I]$ and $D = [I, -e]$, where $I \in \mathbb{R}^{n \times n}$ is the identity matrix and $e \in \mathbb{R}^n$ is the vector of ones [40]. If derivative information is available, Abramson, Audet, and Dennis [8] show how Theorem 2.2.2 can be applied to $D = \{-1, 0, 1\}^n$ to reduce the set of points to be evaluated to a singleton.

In subsequent papers, Lewis and Torczon extended GPS to bound [41] and linearly constrained [42] optimization problems of the form,

$$\begin{aligned} \min_{x \in \mathbb{R}^n} \quad & f(x) \\ \text{s. t.} \quad & l \leq Ax \leq u, \end{aligned} \tag{2.5}$$

where $f : \mathbb{R}^n \to \mathbb{R}$, $A \in \mathbb{Q}^{m \times n}$, and $l \leq u$.

They prove that if f is continuously differentiable and search directions include a set of generators of the cone of feasible directions (with respect to all nearby constraints), then there exists a subsequence of iterates that converges to a point x^* satisfying the Karush-Kuhn-Tucker (KKT) first-order necessary conditions for optimality.

The KKT conditions for linear equality constraints, originally published in 1952 by Kuhn and Tucker [39], but also proved independently by Karush [35] nearly 15 years prior, are given in Theorem 2.2.3 [47, 441] for the linearly constrained case. The first three conditions are referred to as the first-order necessary conditions, while the last is the second-order necessary condition.

Theorem 2.2.3 *If x_* is a local minimizer of f over the set $\{x : Ax \geq b\}$, then for some vector λ_* of Lagrange multipliers*

- $\nabla f(x_*) = A^T \lambda_*$, *or equivalently,* $Z^T \nabla f(x_*) = 0$,
- $\lambda_* \geq 0$,
- $\lambda_*^T (Ax_* - b) = 0$, *and*
- $Z^T \nabla^2 f(x_*) Z$ *is positive semi-definite,*

where Z is a matrix whose columns form a basis for the null-space of the active constraints at x_*.

Convergence behavior of GPS with respect to second-order stationary points is studied in [6] while local convergence rates of GPS are studied in [28]. A thorough review of the more general class of generating set search methods for linearly constrained nonlinear programming problems is given in [38].

2.2.2 Mixed Variable GPS. In [16], Audet and Dennis extend GPS to problems that contain both continuous and categorical variables with bound constraints on the continuous variables; *i.e.*, MVP problems of the form given in (1.1), in which A is the identity matrix. The algorithm they present assumes the objective function f is continuously differentiable when the discrete variables in X^d are fixed. As a result, their algorithm is a generalization of the basic GPS algorithm presented by Lewis and Torczon and reduces to such when the dimension $n^d = 0$ (*i.e.* in the absence of discrete variables).

Kokkolaras, Audet and Dennis [37] apply the MVP algorithm to the design of a thermal insulation system, first considered by Hilal and Boom [32]. They demonstrate a 65% reduction in

the objective function value over previous results that applied other optimization methods. This demonstration shows that the MVP algorithm is highly effective in solving a broad class of engineering problems that were difficult to solve using earlier methods without incorporating engineering intuition into the problem. The Audet-Dennis GPS method for MVP problems was extended further in [50] to problems with random noise in the objective function by adding a ranking and selection scheme.

Two other methods for solving mixed variable problems, one derivative-based and one derivative-free, were developed by Lucidi and Piccialli [44] and Lucidi, Piccialli, and Sciandrone [45], respectively. In their more general framework, trial points are not restricted to lie on a mesh. This allows any suitably chosen derivative-free method (in the case of [45]) to be used instead of pattern search to guarantee convergence to a first-order stationary point. However, it requires a sufficient decrease instead of the simple decrease requirement by pattern search.

2.2.3 GPS extensions. Motivated by the derivative-free nature of GPS, Audet and Dennis [17] introduced a new convergence analysis for linearly constrained problems, in which less smoothness is required on the objective function f. They provide a hierarchy of results that depend on the smoothness of f. Other extension of GPS include the use of a subprocedure that adaptively controls the precision of an approximating objective function [48] and the incorporation of a user-provided scheme to generate points leading to potential objective function decrease [11].

GPS has also been extended to problems with nonlinear constraints. Lewis and Torczon [43] adapt a bound constrained augmented Lagrangian method, first proposed in [23], as way to apply a pattern search algorithm to optimization problems with general constraints and simple bounds. They solve the bound constrained subproblem by replacing the stopping conditions proposed in [23], which require derivatives, with stopping criteria based on mesh size. They demonstrate convergence to a KKT point by linking the size of the pattern in the bound constrained pattern search with the amount of local feasible descent.

Audet and Dennis [19] take a different approach to problems with nonlinear constraints through the development of a filter method [19]. First developed by Fletcher and Leyffer in [29] as a way to globalize sequential linear and quadratic programming, a filter algorithm accepts a step if the objective function or a function measuring aggregate constraint violation is reduced. Audet and Dennis' GPS implementation of a filter method [19] only requires simple decrease in the objective or constraint violation function, but does not guarantee convergence to a first-order KKT point. The extension of [19] to mixed variable problems is presented in [4] which generalizes all of the previous work of Audet and Dennis with convergence results that reduce to previously presented results for the specific class of problems it covers. This approach is applied to a modified version of the problem in [37], in which realistic nonlinear constraints have been added [5].

Motivated by the weaknesses in the convergence theory for the filter GPS algorithm, Audet and Dennis generalize GPS for nonlinearly constrained problems by introducing a new direct search method, known as *mesh adaptive direct search* (MADS) [18]. Unlike GPS, the MADS algorithm does not limit the local exploration of the variable space to a finite number of directions. Instead, MADS ensures an asymptotically dense set of directions. As the convergence theory demonstrates, MADS iterates converge to a limit point satisfying both first-order [18] and second-order [7] necessary or sufficient optimality conditions.

In the following chapters, a detailed description of the mixed variable GPS algorithm is presented, along with its associated convergence theory. Implementation of the algorithm on the LANL problem is discussed, followed by the numerical results and analysis of the algorithm on several test cases of objects.

III. Methodology

This chapter describes the Audet-Dennis [16] class of pattern search algorithms for mixed variable problems with linear constraints, including a summary of convergence results. Much of the description comes from [4, 61-82] and [16]. The algorithm is then applied to the Los Alamos National Laboratory (LANL) quantitative object reconstruction optimization problem and a detailed discussion of the linear constraints and discrete neighbors is presented. Numerical results of this application are discussed in Chapter IV.

As discussed in Chapter I, the LANL object reconstruction problem contains categorical variables. recall, the vector of design variables x is partitioned into its continuous and categorical components; namely, the continuous layer edge boundaries and the discrete number of types of materials. Material types must be selected from a pre-defined list. The number of layers of materials is also treated as a categorical variable, and a change in its value changes the linear constraints and even the dimension of the problem. Because non-integer values of these variables do not make physical sense, temporary relaxations can not be performed. This restriction results is not often seen in other optimization problems.

3.1 GPS for Linearly Constrained MVP Problems

Pattern search is an iterative method that generates a sequence of feasible points with nonincreasing objective function values. At each iteration, the objective function is evaluated at a finite number of points on a mesh in an attempt to find one that decreases the objective function value. The mesh M_k at each iteration is a subset of the domain $\Omega \subset \mathbb{R}^{n^c} \times \mathbb{Z}^{n^d}$.

3.1.1 Mesh Generation. At each iteration, the mesh can be formed as the direct product of the union of a finite number of lattices in $\mathbb{R}^{n^c}$ with the integer space $\mathbb{Z}^{n^d}$, as follows. For each combination $i = 1, 2, \ldots, i_{max}$ of values that the discrete variables may take on, a set of positive

spanning directions D^i is formed by the product

$$D^i = G_i Z_i, \tag{3.1}$$

where $G_i \in \mathbb{R}^{n^c \times n^c}$ is a nonsingular generating matrix and $Z_i \in \mathbb{Z}^{n^c \times |D^i|}$. Then the mesh is the direct product of X^d with a union of a finite number of lattices in X^c centered at the continuous part of the current iterate:

$$M_k = X^d \times \bigcup_{i=1}^{i_{\max}} \{x^c + \Delta_k D^i z : z \in Z_+^{|D^i|}\}. \tag{3.2}$$

In this formulation the number of lattice points is finite and the minimum distance between two distinct mesh points points is proportional to the *mesh size parameter* $\Delta_k > 0$. The mesh size parameter controls the resolution (fineness or coarseness) of the mesh.

3.1.2 Local Optimality. To accommodate both continuous and categorical variables, the GPS algorithm for bound [41] and linearly constrained [42] minimization was extended in [16] and [4], respectively. In doing so, a concept of local optimality was introduced that accounts for variations of both the continuous and categorical variables, but reduces to basic GPS in the absence of categorical variables.

For problems consisting of only continuous variables, local optimality is well-defined: $x_* \in \mathbb{R}^n$ is a local minimizer of $f : \Omega \to \mathbb{R}$ if there exists an $\varepsilon > 0$ such that $f(x_*) \leq f(v)$ for all $v \in B(x_*, \varepsilon) \cap \Omega$, where $B(x_*, \varepsilon)$ is a ball of radius ε centered at x_*. For mixed variable problems, this definition must be augmented to account for discrete variables. This is done by adding the condition [4], $f(x_*) \leq f(y)$ for all $y \in \mathcal{N}(x_*)$, where $\mathcal{N}(x_*)$ is the set of discrete neighbors of x_*. This is formally stated in Definition 3.1.1.

Definition 3.1.1 *A point $x_* = (x_*^c, x_*^d) \in X$ is said to be a local minimizer of f with respect to the set of neighbors $\mathcal{N}(x) \subset X$ if there exists an $\varepsilon > 0$ such that $f(x) \leq f(v)$ for all v in the set*

$$X \cap \bigcup_{y \in \mathcal{N}(x)} \left(B(y^c, \varepsilon) \times y^d \right). \tag{3.3}$$

Definition 3.1.1 not only requires this additional condition, but it also requires that, if $f(y) = f(x_*)$, for all $y \in \mathcal{N}(x_*)$, then $f(y) \leq f(w)$ for all $w \in B(y, \varepsilon) \cap \Omega$. In order to guarantee convergence in the mixed variable case, which is formally defined in Definition 3.1.2, a notion of continuity with respect to the set of discrete neighbors is required for the set-valued function $\mathcal{N} : X \to 2^X$, where 2^X is the power set (or set of all possible subsets) of X. This is given in Definition 3.1.3 [4].

Definition 3.1.2 *Let $X \subseteq (\mathbb{R}^{n^c} \times \mathbb{Z}^{n^d})$ be a mixed variable domain. A sequence $\{x_i\} \subset X$ is said to* converge *to $x \in X$ if, for every $\varepsilon > 0$, there exists a positive integer N such that $x_i^d = x^d$ and $\|x_i^c - x^c\| < \varepsilon$ for all $i > N$. The point x is said to be the* limit point *of the sequence $\{x_i\}$.*

Definition 3.1.3 *The set-valued function $\mathcal{N} : X \subseteq (\mathbb{R}^{n^c} \times \mathbb{Z}^{n^d}) \to 2^X$ is said to be* continuous *at $x \in X$ if, for every $\varepsilon > 0$, there exists $\delta > 0$ such that, whenever $u \in X$ satisfies $u^d = x^d$ and $\|u^c - x^c\| < \delta$, the following two conditions hold:*

1. *If $y \in \mathcal{N}(x)$, then there exists $v \in \mathcal{N}(u)$ satisfying $v^d = y^d$ and $\|v^c - y^c\| < \varepsilon$,*
2. *If $v \in \mathcal{N}(u)$, then there exists $y \in \mathcal{N}(x)$ satisfying $y^d = v^d$ and $\|y^c - v^c\| < \varepsilon$.*

Note that each lattice in (3.2) is expressed as a translation from x_k^c, instead of y_k^c, for some $y_k \in \mathcal{N}(x_k)$. Additionally, the function $\mathcal{N}$ must also be constructed so that every discrete neighbor of the current iterate lies on the current mesh M_k. Both of these conditions are necessary to ensure convergence of the algorithm.

This concept of local optimality requires the user to decide how to define the neighborhood function $\mathcal{N}$. The algorithm will then produce a solution $\hat{x}$, that, under certain conditions, will be locally optimal with respect to its discrete neighbors $\mathcal{N}(\hat{x})$.

3.2 GPS for MVP with Linear Constraints Algorithm

With a newly constructed mesh and local optimality for the mixed variable case defined, it is possible to discuss the algorithm for mixed variable problems with linear constraints given by Abramson [4]. The goal of each iteration of the algorithm is to find a point on the current mesh whose objective value is less than that of the current incumbent. In order to find such a point, the mesh is explored in three phases.

3.2.1 SEARCH *Step.* The first phase, the SEARCH, is simply a search of a finite number of trial points S_k on the mesh M_k where the objective function is evaluated at each point in S_k. This phase is typically more global in nature, and it is free of any any other rules imposed by the algorithm and can be performed anywhere on the mesh. The flexibility in this step allows any strategy (including none) to be specified by the user. One choice is a meta-heuristic such as simulated annealing [36], tabu search [30, 31], or genetic algorithms [26]. Additionally, if f is computationally expensive to evaluate, one common approach is to construct and optimize an inexpensive surrogate function [20] at each SEARCH step. In fact, any other ad/hoc search could be used to improve upon the incumbent.

3.2.2 POLL *Step.* The second phase in the algorithm is the POLL step. Polling occurs whenever the SEARCH step is unsuccessful in finding a point on the current mesh that decreased the objective function value. Polling is done in two steps:

1. polling with respect to the continuous variables at x_k
2. polling on the current set of discrete neighbors $\mathcal{N}(x_k)$.

The first step is identical to that of pattern search algorithms for continuous variables only [17, 51, 41, 42, 40]. Polling with respect to continuous variables requires use of positive spanning sets in $\mathbb{R}^{n^c}$. Let $D_k^i \subseteq D^i$ denote the set of poll directions corresponding to the i-th set of discrete variables for each iteration k. The *poll set* $P_k(x_k)$, centered at x_k, is the set of neighboring mesh points

in the directions D_k^i, while holding the discrete variables fixed; *i.e.*,

$$P_k(x_k) = \{x_k\} \cup \{x_k + \Delta_k(d,0) \in X : d \in D_k^i\} \subset M_k \subset X. \tag{3.4}$$

The notation $(d,0)$ accounts for the partitioning into continuous and discrete variables, where 0 represents no change in the discrete variables. Therefore, $x_k^c + \Delta_k(d,0) = (x_k^c + \Delta_k d, x_k^d)$. If polling with respect to the continuous variables fails to find a point in $P_k(x_k)$ that lowers the objective function value, polling on the current set of discrete neighbors $\mathcal{N}(x_k)$ is performed. The objective function f is evaluated at each of the points in $P_k(x_k)$ until a lower objective function is found or until all points have been evaluated.

3.2.3 EXTENDED POLL *Step.* In the event that both the poll set and set of discrete neighbors fails to find improvement in the objective function value, the algorithm performs the third step, called EXTENDED POLL, before declaring the iteration unsuccessful [16]. In this step, additional polling is performed around each discrete neighbor point $y \in \mathcal{N}(x_k)$, whose objective function value was only a small amount greater than that of the incumbent. This is done because $y \in \mathcal{N}(x_k)$ is a promising point and a poll around y may produce a better objective function value than the incumbent. The EXTENDED POLL step is performed whenever $f(y_k) < f(x_k) + \xi_k$, where the *extended poll trigger* ξ_k satisfies $\xi_k \geq \xi$ for a fixed $\xi > 0$. The values for ξ_k are often set as a percentage of the objective function value at the current iterate [4]. Large ξ values should yield a better local minimizer, but would generate more EXTENDED POLLS, resulting in an increase of function evaluations.

For each iteration k, the set of extended poll points for a discrete neighbor $y \in \mathcal{N}_k$, denoted ε_y, is evaluated and forms the *extended poll set* given by

$$\mathcal{N}_k = \bigcup_{y \in \mathcal{N}_k^{\xi}} \varepsilon(y) \tag{3.5}$$

where $\mathcal{N}_k^{\xi} = \{y \in \mathcal{N}(x_k) : f(x_k) \leq f(y) \leq f(x_k) + \xi_k\}$. Polling then begins around the continuous neighbors of y_k in a sequence $\{y_k^j\}_{j=1}^{J_k}$ and continues until either all continuous neighbors have been evaluated or until a point is found that decreases the objective function value. The *endpoint* of the EXTENDED POLL step, is denoted as z_k.

A visual representation of the POLL and EXTENDED POLL steps is shown in Figure 3.1 in the case of one discrete and two continuous variables. The current iterate x_k lies on the middle plane and is surrounded by the continuous poll points u, v, and w. The upper and lower planes contain the points y_1^0 and y_2^0, respectively, which represents discrete neighbors. These discrete neighbors themselves surrounded by continuous poll points, that may be evaluated during the EXTENDED POLL step.

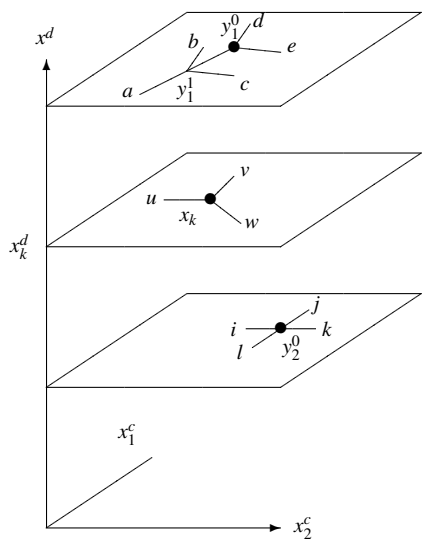

$$P_k(x_k) = \{u, v, w\}$$

$$\mathcal{N}(x_k) = \{x_k, y_1^0, y_2^0\}$$

$$f(x_k) \leq f(y_1^0) < f(x_k) + \xi_k < f(y_2^0)$$

$$\mathcal{X}_k(\xi_k) = \{y_1^1\} \cup \{a, b, c\}$$

Figure 3.1: Construction of the Poll and Extended Poll Sets

3.2.4 Updating the Mesh. The outcomes of evaluating the points can be described as follows, where S_k is the set of SEARCH points at iteration k [4]:

Definition 3.2.1 *If $f(y) < f(x_k)$ for some $y \in S_k \cup P_k(x_k) \cup \mathcal{N}(x_k) \cup \mathcal{X}(\xi_k)$, then y is said to be an* improved mesh point.

Definition 3.2.2 *If $f(x_k) \leq f(y)$ for all $y \in P_k(x_k) \cup \mathcal{N}(x_k) \cup \mathcal{X}_k(\xi_k)$, then x_k is said to be a* mesh local optimizer.

If the SEARCH, POLL, or EXTENDED POLL step is successful in finding an improved mesh point, it becomes the new incumbent x_{k+1}, in which case, the mesh is either retained or coarsened according to the following rule [9],

$$\Delta_{k+1} = \tau^{m_k^+} \Delta_k, \tag{3.6}$$

where $m_k^+ \in \{0, 1, \ldots, m_{\max}\}$ for some $m_{\max} \in \mathbb{Z}_+$ and $\tau > 1$ is rational and fixed over all iterations. This formulation allows the mesh to be retained at the same size when $m_k^+ = 0$. Mesh coarsening does not affect theoretical convergence properties. It can slow or speed convergence, but it can also cause the algorithm to skip over a local minimum and find a better one [9] .

If the SEARCH, POLL, and EXTENDED POLL steps are unsuccessful, then the incumbent is a mesh local optimizer and is retained (*i.e.* $x_{k+1} = x_k$) and the mesh must be refined by the rule [9],

$$\Delta_{k+1} = \tau^{m_k^-} \Delta_k, \tag{3.7}$$

where $m_k^- \in \{m_{min}, m_{min+1}, \ldots, -1\}$. The GPS algorithm is for linearly constrained MVP problems is fully described in Figure 3.2.

3.2.5 Treating Linear Constraints. To treat linear constraints, infeasible points are simply ignored and not evaluated by the objective function. To guarantee convergence, the only additional requirement is that polling directions must be chosen that conform to the geometry of the linear constraint boundaries and that these directions are used an infinite number of times [4]. Definition 3.2.3 [17] abstracts the idea of conforming directions.

Mixed Variable Pattern Search with Linear Constraints

Initialization: Let $x_0 \in X$ satisfy $f(x_0) < \infty$. Set $\Delta_0 > 0$ and $\xi > 0$.
For $k = 0, 1, 2, \ldots$, perform the following:

1. Set extended poll trigger $\xi_k \geq \xi$.
2. SEARCH **step:** Employ some finite strategy seeking an improved mesh point; *i.e.*, $x_{k+1} \in M_k$ such that $f(x_{k+1}) < f(x_k)$.
3. POLL **step:** If the SEARCH step does not find an improved mesh point, evaluate f at points in $P_k(x_k) \cup \mathcal{N}(x_k)$ until an improved mesh point x_{k+1} is found (or until complete).
4. EXTENDED POLL **step:** If the SEARCH and POLL steps does not find an improved mesh point, evaluate f at points in $\mathcal{X}_k(\xi_k)$ until an improved mesh point x_{k+1} is found (or until complete).
5. **Update:** If SEARCH, POLL, or EXTENDED POLL finds an improved mesh point,
   Update x_{k+1}, and set $\Delta_{k+1} \geq \Delta_k$ according to Equation(3.6);
   Otherwise, set $x_{k+1} = x_k$, and set $\Delta_{k+1} < \Delta_k$ according to Equation(3.7).

Figure 3.2: MVP GPS Algorithm

Definition 3.2.3 *A rule for selecting the positive spanning sets $D_k = D(k, x_k) \subseteq D$* conforms to *$\Omega \subseteq \mathbb{R}^n$ for some $\varepsilon > 0$, if at each iteration k and for each y in the boundary of Ω for which $\|y - x_k\| < \varepsilon$, the tangent cone $T_\Omega(y)$ is generated by nonnegative linear combinations of a subset of the columns of D_k.*

The *tangent cone*, $T_\Omega(x)$ to Ω is defined by $T_\Omega(x) = cl\{\mu(w - x) : \mu \geq 0, w \in \Omega\}$. It is the set of feasible directions at $x \in \mathbb{R}^n$ [17]. Figure 3.3 shows positive spanning directions that conform to the geometry of the nearby linear constraint boundaries.

Lewis and Torczon [42] show how to generate these directions using linear algebra tools, so that if chosen properly, convergence to an appropriate stationary point can be ensured. A summary of their algorithm is found in Figure 3.4 [4] This algorithm works as long as no degenerate conditions exist at the limit point of the algorithm. Methods for handling degeneracy are described in [10].

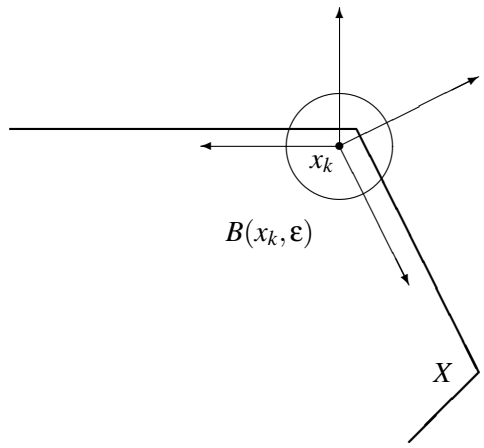

Figure 3.3: Directions that Conform to the Geometry of X

3.3 Convergence of the GPS Algorithm for MVP Problems

We now present the convergence theory for the algorithm given in Figure 3.2. In order to present a hierarchy of results that depend on the smoothness of f, we first need some preliminary definitions and theorems from the Clarke nonsmooth calculus [22].

Definition 3.3.1 *A function $f : Y \subseteq \mathbb{R}^n \to \mathbb{R}$ is said to satisfy a* Lipschitz condition *on Y if there exists a scalar $L \geq 0$ such that, for all x, x' in Y,*

$$|f(x) - f(x')| \leq L\|x - x'\|. \tag{3.8}$$

The function f is said to be Lipschitz near *$x \in Y$ if, for some $\varepsilon > 0$, f satisfies a Lipschitz condition on $B(x, \varepsilon)$, where $B(x, \varepsilon)$ is an open ball of radius ε centered at x.*

Algorithm for Computing Conforming Directions D_k

- Set $\varepsilon_k \geq \varepsilon > 0$. Assume the current iterate x_k satisfies $\ell \leq Ax_k \leq u$.
- While $\varepsilon_k \geq \varepsilon$, do the following:
  1. Let $I_\ell(x_k, \varepsilon_k) = \{i : Ax - \ell \leq \varepsilon_k\}$
  2. Let $I_u(x_k, \varepsilon_k) = \{i : u - Ax \leq \varepsilon_k\}$
  3. Set V denote the matrix whose columns are formed by all the members of the set $\{-a_i : i \in I_\ell(x_k, \varepsilon_k)\} \cup \{a_i : i \in I_u(x_k, \varepsilon_k)\}$, where a_i^T denotes the i-th row of A.
  4. If V does not have full column rank, then reduce ε_k just until $|I_\ell(x_k, \varepsilon_k)| + |I_u(x_k, \varepsilon_k)|$ is decreased, and return to step 1.
- Set $B = V(V^TV)V^{-1}$ and $N = I - V(V^TV)V^{-1}V^T$.
- Set $D_k = [N, -N, B, -B]$.

Figure 3.4: Algorithm for Generating Conforming Directions

Definition 3.3.2 (Clarke) *Let $f : \mathbb{R}^n \to \mathbb{R}$ be Lipschitz near a given point x. The* generalized directional derivative *of f at x in the direction v is given by*

$$f^\circ(x; v) := \limsup_{y \to x, t \downarrow 0} \frac{f(y + tv) - f(y)}{t}, \tag{3.9}$$

where t is a positive scalar.

Definition 3.3.3 *The function $f : \mathbb{R}^n \to \mathbb{R}$ is said to be* strictly differentiable *at x if, for all $v \in \mathbb{R}^n$,*

$$\lim_{y \to x, t \downarrow 0} \frac{f(y + tv) - f(y)}{t} = \nabla f(x)^T v. \tag{3.10}$$

Additionally, to ensure convergence, the following assumptions are made.

A1: All iterates $\{x_k\}$ produced by the algorithm lie in a compact set.
A2: For each fixed set of discrete variable values x^d, the corresponding set of directions $D^i = G_i Z_i$, includes tangent cone generators for every point in $X^c(x^d)$.
A3: The rule for selecting directions D_k conforms to X^c for some $\varepsilon > 0$.
A4: The discrete neighbors always lie on the mesh; i.e., $\mathcal{N}(x_k) \subset M_k$ for all k

3.3.1 Mesh Size Behavior and Limit Points. Torczon [51] shows that, under Assumption A1 and the additional assumptions of a continuously differentiable objective function, the mesh size becomes arbitrarily small and the mesh size parameters are bounded above by a positive constant that is independent of the iteration. This idea is formally presented in Theorem 3.3.4 and reproved in [16] and [4] for MVP problems.

Theorem 3.3.4 *The mesh size parameters satisfy* $\liminf_{k \to +\infty} \Delta_k = 0$.

The following definitions, adapted from Audet and Dennis [17] are needed in order redefine the concept of a limit direction for mixed variable spaces.

Definition 3.3.5 *A subsequence of GPS mesh local optimizers $\{x_k\}_{k \in K}$ (for some subset of indices K) is said to be a* refining subsequence *if $\{\Delta_k\}_{k \in K}$ converges to zero.*

Definition 3.3.6 *Let $\{v_k\}_{k \in K}$ be either a refining subsequence or a corresponding subsequence of extended poll endpoints, and let $\hat{v}$ be a limit point of the subsequence. A direction $d \in D$ is said to be a* refining direction *of $\hat{v}$ if $w_k = v_k + \Delta_k(d, 0) \in X$ and $f(v_k) \leq f(w_k)$ for infinitely many $k \in K$.*

Additionally, Theorem 3.3.7 [16] establishes the existence of limit points of interest. This demonstrates the existence of a limit point of subsequences of interest. Finally, they establish the local optimality conditions the limit point $\hat{x}$ satisfies with respect to the discrete variables.

Theorem 3.3.7 *Let $L_X(x_0) = \{x \in X : f(x) \leq f(x_0)\}$. There exists a point $\hat{x} \in L_X(x_0)$ and a refining subsequence $\{x_k\}_{k \in K}$ (with associated index set K) such that $\lim_{k \in K} x_k = \hat{x}$. Moreover, if $\mathcal{N}$ is continuous at $\hat{x}$, then there exists $\hat{y} \in \mathcal{N}(\hat{x})$ and $\hat{z} = (\hat{z}^c, \hat{y}^d) \in X$ such that*

$$\lim_{k \in K} y_k = \hat{y} \quad \textit{and} \quad \lim_{k \in K} z_k = \hat{z},$$

where each $z_k \in X$ is the endpoint of the EXTENDED POLL *step initiated at $y_k \in \mathcal{N}(x_k)$.*

A visual representation of these limit points is given in Figure 3.5 [4]. The lower plane of the figure shows the sequence of improving iterates $\{x_k\}$ converging to the limit point $\hat{x}$. The upper plane shows the sequence of discrete neighbors $\{y_k\}$ and the sequences of extending poll points $\{y_k^i\}$, $j = 1, \ldots, J_k$, where $z_k = y_k^{J_k}$, and $\hat{y}$, $\bar{y}$, and $\hat{z}$ are the corresponding limit points.

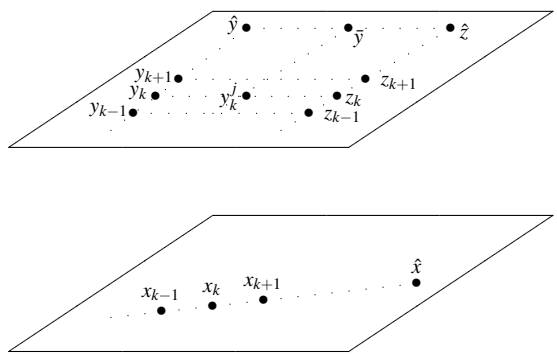

Figure 3.5: Limit Points of Iterates and Extended Poll Centers.

3.3.2 Main Convergence Properties. The remainder of the theorems presented show convergence to points satisfying certain optimality conditions under the weaker assumption of strict differentiability of the objective function f. If the objective function f is Lipschitz near the limit point of a refining subsequence, Theorem 3.3.8 and Theorem 3.3.9 establishes the directional optimality condition [4].

Theorem 3.3.8 *Let $\hat{x}$ be a limit point of a refining subsequence. Under Assumptions A1–A3, if f is Lipschitz near $\hat{x}$ with respect to the continuous variables, then $f^{\circ}(\hat{x};(d,0)) \geq 0$ for all limit directions $d \in D$ of $\hat{x}$.*

Theorem 3.3.9 *Let $\hat{x}$, $\hat{y} \in \mathcal{N}(\hat{x})$, and $\hat{z}$ be defined as in the statement of Theorem 3.3.7, with $\mathcal{N}$ continuous at $\hat{x}$, and let $\xi > 0$ denote a lower bound on the extended poll triggers ξ_k for all k. If $f(\hat{y}) < f(\hat{x}) + \xi$ and f is Lipschitz near $\hat{z}$ with respect to the continuous variables, then $f^{\circ}(\hat{z};(d,0)) \geq 0$ for all limit directions $d \in D$ of $\hat{z}$.*

Theorem 3.3.10 and Theorem 3.3.11 demonstrate that if the objective function f is strictly differentiable at $\hat{x}$ and the Assumption A3 holds, $\hat{x}$ and $\hat{z}$ satisfy first-order necessary conditions for optimality with respect to the continuous variables [4].

Theorem 3.3.10 *Let $\hat{x}$ be a limit point of a refining subsequence with limit directions $D(\hat{x})$, and let f be strictly differentiable at $\hat{x}$. Then under Assumptions A1–A3, $\hat{x}$ is a KKT point with respect to the continuous variables. Furthermore, if $X^c = \mathbb{R}^{n^c}$ or if $\hat{x}^c$ lies in the interior of X^c, then $\nabla^c f(\hat{x}) = 0$.*

Theorem 3.3.11 *Let $\hat{x}$, $\hat{y} \in \mathcal{N}(\hat{x})$, and $\hat{z}$ be defined as in the statement of Theorem 3.3.7, with $\mathcal{N}$ continuous at $\hat{x}$, and let $\xi > 0$ denote a lower bound on the extended poll triggers ξ_k for all k. Let $D(\hat{z})$ be the limit directions of $\hat{z}$, and suppose f is strictly differentiable at $\hat{z}$ with respect to the continuous variables. If $f(\hat{y}) < f(\hat{x}) + \xi$, then under Assumptions A1–A4, $\hat{z}$ is a KKT point with respect to the continuous variables. Furthermore, if $X^c = \mathbb{R}^{n^c}$ or $\hat{z}^c$ lies in the interior of X^c, then $\nabla^c f(\hat{z}) = 0$.*

Additionally, Theorem 3.3.12 [16] establishes local optimality of $\hat{x}$ with respect to its discrete neighbors, in accordance with Definition 3.1.1.

Theorem 3.3.12 *Let $\hat{x}$ and $\hat{y} \in \mathcal{N}(\hat{x})$ be defined as in the statement of Theorem 3.3.7, such that $\mathcal{N}$ is continuous at $\hat{x}$. If f is continuous at $\hat{x}$ and $\hat{y}$ with respect to the continuous variables, then $f(\hat{x}) \leq f(\hat{y})$.*

3.4 GPS Algorithm Applied to the LANL Problem

The development of the GPS algorithm for mixed variable problems with linear constraints and the associated convergence theory in [4] allows for proper evaluation of the LANL problem because the algorithm can handle both continuous and discrete variables. We now describe the application of GPS to the LANL problem of quantitatively reconstructing cylindrically objects using x-ray tomography.

3.4.1 Problem Formulation. To quantitatively describe the object composition, comparisons must be made between likely object configurations and the data to determine how well the configuration matches the data. The goal of LANL researchers is to find configuration that best match the data given certain constraints. The variables for this problem include the number of material layers, the material composition of each layer, and the outer edge location of each material layer. The edge location of each layer exists at the termination of one material type and the start of a different material type. Furthermore, it is assumed that the material layers are concentric circles, meaning their radius r is constant as a function of radial angle θ. Due to the physical interactions involved in x-ray radiography, discussed in Chapter II, as well as noise involved in the process, a perfect match is generally impossible. As a result, the GPS algorithm will determine the most likely configuration given the data. A more specific model of the optimization problem is given as

$$\begin{aligned} \min_{(n,x,m)\in X} \quad & f(n,x,m) \\ \text{s. t.} \quad & l \leq Ax \leq u, \end{aligned} \tag{3.11}$$

where n is the number of material layers, $x \in \mathbb{R}^n$ is a vector whose i-th component is the edge location of the i-th material layer, and $m \in M^n$ is the material composition of the object, where m_i represents the i-th material type, whose edge location corresponds to x_i, and M denotes the finite set of possible material types. Thus in this formulation x and $\{n,m\}$ play the role of x^c and x^d, respectively, from (2.5).

The feasible region X is defined by the following linear and categorical constraints:

$$n \in \{n_{\min}, \ldots, n_{\max}\} \tag{3.12}$$

$$m \in M^n \tag{3.13}$$

$$x_n \leq L - \delta \tag{3.14}$$

$$x_{i+1} > x_i + \delta,\ i = 1, \ldots, n \tag{3.15}$$

$$l \leq Ax \leq u. \tag{3.16}$$

In these constraints, L is the distance from the center of the object to the recording radiograph, δ is the minimum layer thickness, l and u are vectors of lower and upper bounds, respectively, on the material edge locations x, and A is a rational coefficient matrix. It is important to note at this point that the object size L is a known quantity. However, since the object in question is assumed to be cylindrically symmetrical, it is impossible to place the planar recording radiograph exactly at the physical edge of the object. As a result, the x-rays must transmit through a known transmission material layer m_{n+1} whose edge location x_{n+1} is fixed. For example, x-rays taken under normal atmospheric conditions have a transmission layer of air. This transmission layer is not considered by any other part of the MVP algorithm, except in the objective function calculation and accounts for the $L - \delta$ restriction on x_n in (3.12).

The dimensionality of this problem and the presence of categorical variables makes it difficult to solve using optimization methods other then GPS because the dimensions of the vectors x, and m depend on n. As a result, for every value of n, there are n other categorical variables and n continuous variables, resulting in a total of $2n + 1$ variables.

3.4.2 Objective Function. An ongoing effort at LANL is to determine an objective function that adequately accounts for the physical interactions of scattering, experimental setup including x-ray source used, and adequate modeling of the measurement process. As a result, several objective functions are currently being considered for each of the experimental setups described in

Chapter IV; however, all of the objective functions are currently of the form,

$$f(u) = \frac{\|Pu - d\|_2}{\sqrt{\frac{L}{w}}}, \tag{3.17}$$

where the operator P is the discretized Abel projection matrix, w is the radiograph pixel width (square pixels are assumed), $u \in \mathbb{R}^{\frac{L}{w}}$ is a pixelized version of the object and is a function of the edge locations x and material types m, and $d \in \mathbb{R}^{\frac{L}{w}}$ is the data from the radiograph. The P operator is scaled to the unit radiograph data pixel width w. Therefore, P is an $\frac{L}{w} \times \frac{L}{w}$ matrix that reconstructs the object from u at the maximum resolution that can be ascertained from the radiograph data and is a linear geometric projection of a circularly discretized object. Regardless of the form the objective function takes, the goal is to find the most likely recreation of the object's composition that matches the data from radiograph.

3.4.3 Linear Constraints. Although the constraints from (3.11) only apply to the continuous variables, the material layer edge locations x, they are also functions of the number of material layers n, a categorical variable. As a result, changes in the categorical variables may necessitate a change in the continuous variables. The linear constraints on material edge layer locations are specified in each problem by the user through a fixed minimum thickness δ of each material layer, as well as the maximum edge location of the outermost material layer $L - \delta$.

In order to obey the linear constraints, it is useful to compare the edge locations of adjacent layers. The thickness of material layer m_i is computed simply as the difference in edge locations; namely $x_i - x_{i-1}$, $i = 1, 2, \ldots, n$, where $x_0 = 0$ and $x_n \leq L - \delta$. Additionally, the lower and upper bound on the innermost and outermost materials layer must be be taken into account. This results in the formation of a rational coefficient matrix $A \in \mathbb{R}^{(n+1)\times n}$ with ones on the diagonal and negative ones on the sub-diagonal, and with the $n+1$ row containing all zeroes except for a one in the last

entry. For example, if $n = 4$, then

$$A = \begin{bmatrix} 1 & 0 & 0 & 0 \\ -1 & 1 & 0 & 0 \\ 0 & -1 & 1 & 0 \\ 0 & 0 & -1 & 1 \\ 0 & 0 & 0 & 1 \end{bmatrix}. \tag{3.18}$$

Under this formulation, $l \in \mathbb{R}^{n+1}$ can be simply formed with δ down the entire column vector with the exception of the last row which fixes the minimum edge location of the outermost material layer to ensure each layer satisfies the minimum thickness. For example, if $\delta = 3$ and $n = 4$, then

$$l = \begin{bmatrix} 3 \\ 3 \\ 3 \\ 3 \\ 12 \end{bmatrix}. \tag{3.19}$$

On the other hand, $u \in \mathbb{R}^{n+1}$ takes on a more complex form to limit the maximum thickness of each layer. It must take into account the maximum edge location of the outermost (non-transmission) material layer as well as maximum layer thickness that preserves minimum layer thicknesses. As a result, u is given as a column vector with each component defined by $L - \delta n$. For example, if $\delta = 3$, $n = 4$ and $L = 100$, then

$$u = \begin{bmatrix} 88 \\ 88 \\ 88 \\ 88 \\ 97 \end{bmatrix}. \tag{3.20}$$

3.4.4 Discrete Neighbors. Recall from Definition 3.1.1 that a set of discrete neighbors must be defined by the user. Thus, when a solution to a MVP problem is found, it is always with respect to this set of discrete neighbors. A general neighborhood structure where every set of discrete variable is a neighbor of all other sets of discrete neighbors may result in a more global solution, but at a very high computational cost [4]. However, underlying knowledge of the physical processes involved in the problem allows restriction of the size of the set of neighbors that must be examined at each iteration. As a result, there exists the possibility of significant savings in computational cost and time, but may result in a more localized optimizer with a higher objective function value.

The neighborhood structure of the discrete neighbors is perhaps the most interesting aspect of the MVP GPS application to the LANL problem. It takes into account inherent properties of Abel transform x-ray tomography, as well as known properties of the material types. Three types of neighbors were permitted:

1. Swapping any layer with a material of a different type
2. The deletion of any single material layer
3. The addition of a single material layer between two existing layers

These neighbors were chosen to limit the size of the set of discrete neighbors and to ensure that each neighbor was a mesh point. Otherwise, if the set of neighbors is not restricted in this way, then it would contain $\sum_{n=1}^{n_{\max}} m^n$ points at a given point, which would need to be evaluated during every unsuccessful iteration. This number grows very fast, even for modest values of m and n.

In order to take advantage of underlying knowledge of the physical processes involved in the problem, a user-defined adjacency matrix was utilized. The matrix, is square and binary, and each row or column represents a material type. A value of 1 in the $(i, j)^{th}$ element means that material i is adjacent to material j. It is likely that a user would desire an adjacency matrix that is fully connected. A fully connected matrix implies that any material can be reached from any other material either directly or through other materials [1]. Adjacent materials may be thought of

as materials that may be confused for one another in the current object configuration. To prevent redundant neighbors, a material is not considered adjacent to itself. For example, lead and iron affect the scattering and attenuation of x-ray photons as they pass through these materials in similar manners. Thus, it is easy to confuse lead and iron when analyzing the results of a radiograph. As a result, these materials may be considered adjacent; however, since lead is not easily confused with air, they are not considered adjacent to each other. Information in the adjacency matrix was utilized in each of the three types of neighbors examined in order to limit the size of the set of discrete neighbors.

In addition to an adjacency matrix, information about the process of Abel transform x-ray tomography was used to determine the order in which the neighbors that were evaluated. Changes to the outside material layers affect more of the data than the inside layers. As a result, neighbors with changes to the outside material layers were always evaluated before those with changes to internal material layers because more change in the objective function is expected. For each type of neighbor examined, there are unique considerations, which are due to the adjacency matrix, the presence of the transmission material, and the minimum and maximum number layers permitted. As such, each type of neighbor considered will be discussed in detail.

A swap of a material involves replacing one material in a layer with another material from the material library M while layer thicknesses remain fixed. It is the simplest of neighbor types and has the least restrictions. The only restriction on the swap is that the new material must be adjacent to that of the old material, as defined by the adjacency matrix. Additionally, if the outermost layer m_n is to be swapped, the material of the transmission layer m_{n+1} cannot be considered.

The deletion of a material layer is slightly more complex than a simple material swap. Any layer m_i maybe considered for deletion if either the interior or exterior material layer, m_{i-1} or m_{i+1}, respectively, is adjacent to the material layer being considered, and provided that the current number of material layers n is greater than the minimum number of material layers $n_{\min}$. However, if outermost material layer m_n is considered and the interior material layer m_{n-1} is of the same material type as the transmission layer, both the outermost material layer m_n and the interior material

layer m_{n-1} will be deleted. In the case of deletion of material layer m_i, the corresponding edge location x_i will also be deleted. The material layer exterior m_{i+1} simply absorbs the thickness of the deleted material layer. Again, material layer deletion is considered first at material layer m_n and works interior to material layer m_1.

The addition of a material layer is the most complex type of neighbor because it requires the addition of an edge location. All materials in the library M are considered for addition exterior to material layer m_i, as long as the material being considered is adjacent to either material layer m_i or m_{i+1}, and provided that the current number of material layers n is less than the maximum number of material layers $m_{\max}$. The new edge location is simply located halfway between the edge locations of the interior and exterior layers, x_i and x_{i+1}, respectively. If the material layer being added is exterior to the outermost layer m_n, the transmission material layer m_{n+1} is considered for adjacency, and L is considered for the exterior layer location.

Although specific values were used in this section as demonstrative examples to further the understanding the linear constraints and the adjacency matrix, Chapter IV contains descriptions of the various test cases examined, the parameters specified by LANL for these test cases, and the associated numerical results provided by the NOMADm implementation of the algorithm described in this chapter.

IV. Numerical Results

To demonstrate the effectiveness of the GPS on the linearly constrained MVP LANL problem is demonstrated by testing the approach on several sets of data using a MATLAB® implementation of the algorithm from Chapter III . Each data test set was generated using a simulation of a radiograph with simplifications and assumptions made on the test conditions. With each successive simulation model, these simplifications were relaxed. By slowly increasing the "realism" of the data, adjustments to parameters were made and the effects of adding back in realistic conditions on the performance of the GPS algorithm were examined.

Since a large majority of the simulated conditions were common among the test sets, it is appropriate to first discuss these common conditions and note the differences in the assumptions for each test set examined only when necessary.

4.1 Algorithm Implementation

The algorithm described in Chapter III was executed using a MATLAB® implementation of the GPS algorithm, called NOMADm, that can accommodate mixed variables and linear constraints [3]. NOMADm requires up to five MATLAB® function files as follows:

1. a function defining the objective function f,
2. a function that specifies the initial iterate,
3. a function that returns the bound vectors l and u and coefficient matrix A that define the linear constraints $l \leq Ax^c \leq u$,
4. a function defining the set of discrete neighbors, and
5. a function that stores any user-defined parameters needed by the other files.

The functions constructed for the LANL problem are given in Appendix B. Researchers at LANL developed the function files needed to specify the objective function given in (3.11). In setting up these files, the following was provided by LANL;

- object test cases
- discretized Abel transform P
- radiograph data d
- radiograph pixel size w
- objective function to be used,
- library of possible materials M and associated material parameters needed by the objective function
- adjacency matrix used to define neighboring materials
- minimum number of material layers permitted n_{min}
- maximum number of material layers permitted n_{max}
- minimum thickness of a material layer
- initial iterate guess, consisting of layer materials and edge locations

4.2 Data generation

4.2.1 Experimental Conditions. Simulated radiograph data were used to allow for simplifications and assumptions made to test the effectiveness of the algorithm at different levels of realism. A x-ray source's intensity and photon energies are a function of beam and experimental condition geometry making material identification difficult. As a result, a simulated idealized case of a cygnus x-ray source was used; this produces a planar parallel beam of uniform intensity and photon energies. Additionally, a 4 centimeter (cm) wide perfect radiograph detector located 10 cm from the center of the object was assumed with a detector pixel size of 200 microns (μm). (A perfect radiograph detector is one that is 100% efficient at collecting photons at any energy level.) These assumptions allow the simulations to be independent of beam and experimental setup geometry. Additionally, as discussed in Chapter II, particles subject to scattering and changes in energy can make object reconstruction difficult. As a result, these particles were initially ignored. Finally,

all simulations assumed that the objects were x-rayed in normal atmospheric conditions, resulting in a transmission layer of air.

A cygnus x-ray source was used for the simulated radiographs because the energy spectrum and how it is attenuated by materials is well understood. However, the cygnus x-ray source is polychromatic and produces photons in energy levels that vary over a spectrum from 0 to 2.4 MeV. For this problem, relative beam intensity energy level is used to generate the radiographs, and the polychromatic x-ray beam is represented as a linear combination of relative intensities of 23 monochromatic beams.

Radiographs for the polychromatic cygnus x-ray source were generated in one of two ways. Under the simplifying assumptions, a 1-dimensional radiograph of transmission values for a particular energy level of the x-ray source can be directly calculated. These monochromatic radiographs are produced at several energy levels, and the polychromatic radiograph is formed from the summation of the monochromatic beam radiographs [14]. Simulated Poisson noise was then added, based on particle count estimates from other experiments [14] and was used to generate simulated radiographs.

Another way to produce simulated radiographs is to use a Monte Carlo approach of sending one x-ray photon through the object at a time. To generate these radiographs, the Monte Carlo Particle Transport Code (MCNP), developed at LANL, was used. This code is capable of handling detailed physical treatments of the interactions of the x-ray photons and charged particles in the material layers of the object. As a result, high-fidelity simulated radiographs of actual experimental conditions, that include scattering, an accurate model of the x-ray source, and experiment geometry, can be obtained. Two sets of radiographs were generated using MCNP; one that includes scattered photons and one that does not. In the second case, photons which underwent a scattering event between the simulated cygnus x-ray source and the 100% effective detector were simply removed, producing a false radiograph with no scattering.

The MCNP simulations provide a 2-dimensional integrated energy radiograph. One dimensional data was extracted from the radiographs by considering only a horizontal slice of the data centered on the object. The values are then converted to a relative transmission value based on the background level estimate from the radiographs that did not include scattering. These radiographs naturally contain Poisson-like noise. The noise is not exactly Poisson because the transmission values are integrated energy values that depend on the source.

From these test sets, each object optimization test case is generated. Each case includes the radiograph data d, the pixel size w, and the discetized Abel transform P, which is the linear geometric projection for a circularly symmetric discretized object, subject to a plane parallel photon beam from the cygnus x-ray source.

4.2.2 Materials. To keep the dimensionality of the problem manageable, researchers at LANL limited the possible number of material types to nine. Seven of these materials were selected to be representative of a larger group of materials that all possess similar physical attributes and will interact with x-ray photons in a similar manner. Table 4.1 shows the materials selected, their abbreviations which will be used throughout this section, and the material class they represent. Copper (Cu) and Iron (Fe) were deliberately chosen to represent very similar material groups in order to test the algorithm's ability to distinguish between two different materials with very similar physical attributes.

The adjacency matrix used to help define the discrete neighborhood function was provided by LANL. Shown in Table 4.2, this matrix was developed based on prior experience of the researchers who are familiar with the behavior of the materials exposed to x-ray photons and helps to limit the size of the set of discrete neighbors at each trial point.

4.2.3 Object Test Sets. Two test sets of object configurations were examined. The first test set included six objects, each with three layers of materials whose composition consisted of Fe, Be, and Peth with material edge locations at 1.0, 2.0, and 3.0 cm, surrounded by a transmission

Table 4.1: Possible Materials.

Material	Abbreviation	Representative class
Air	Air	Voids and unpressurized gases
Polyethylene	Peth	Light plastics and organic materials
Beryllium	Be	Specifically beryllium
Teflon	Teflon	Dense plastics
Aluminum	Al	Specifically aluminum
Stainless Steel	Fe	Iron-like medium density metals
Copper	Cu	Other medium density metals
Lead	Pb	Heavy metals
Uranium	U	Very heavy metals

Table 4.2: Adjacency Matrix.

	Air	Peth	Be	Teflon	Al	Fe	Cu	Pb	U
Air	0	1	1	1	1	0	0	0	0
Peth	1	0	1	1	1	0	0	0	0
Be	1	1	0	1	1	0	0	0	0
Teflon	1	1	1	0	1	1	1	0	0
Al	1	1	1	1	0	1	1	0	0
Fe	0	0	0	1	1	0	1	1	1
Cu	0	0	0	1	1	1	0	1	1
Pb	0	0	0	0	0	1	1	0	1
U	0	0	0	0	0	1	1	1	0

Table 4.3: Test Set 1 Object Configuration.

Test Case	Material	Edge Location (cm)
1a.	[Fe, Be, Peth]	[1.0, 2.0, 3.0]
1b.	[Fe, Peth, Be]	[1.0, 2.0, 3.0]
1c.	[Be, Fe, Peth]	[1.0, 2.0, 3.0]
1d.	[Be, Peth, Fe]	[1.0, 2.0, 3.0]
1e.	[Peth, Fe, Be]	[1.0, 2.0, 3.0]
1f.	[Peth, Be, Fe]	[1.0, 2.0, 3.0]

layer of Air. All six possible combinations of these materials in different order (see Table 4.3) were tested. These objects are ideal for testing the GPS algorithm because Fe, Be and Peth are significantly different from each other in the way they attenuate a cygnus x-ray source. Additionally, the equal spacing of material edge locations at 1.0, 2.0, and 3.0 cm makes the discrete neighbors formed by adding a material highly effective. For example, if the algorithm is able to accurately locate the edge of material located at or near 2.0 cm, the addition of a material would place the edge locations at or near 1.0 and 3.0 cm. Because of this, results from this test set were used to tune the algorithm parameters values in the NOMADm software.

The second test set includes ten objects whose composition was randomly generated. The number of material layers was randomly selected between $n_{\min}$ and $n_{\max}$ and each layer's material was randomly selected from the material library, in a way that ensured no two adjacent layers had the same materials. Edge locations were randomly generated between 0.1 and 3.9 cm, with a safeguard to prevent any layer's thickness from falling below the threshold of $\delta = 0.1cm$. The resulting test set is described in Table 4.4 and is representative of the composition on an unknown object.

4.2.4 Objective Functions. A single objective function is used but two different material descriptions are utilized. The first material description uses a single material attenuation coefficient value, $a(m)$, for the entire spectrum of the x-ray energy source to describe each material type. Recall that, the x-ray source produced photons over a spectrum of energy levels and each mate-

Table 4.4: Test Set 2 Object Configuration.

Test Case	Material	Edge Location (cm)
2a.	[Fe, Teflon, Fe]	[1.3973, 1.7028, 2.7225]
2b.	[Be]	[2.4927]
2c.	[Be, Fe]	[1.7136, 2.4441]
2d.	[Air, Al]	[3.6109, 3.8152]
2e.	[Be, Air, Teflon, Be]	[0.2379, 0.8433, 1.9587, 3.4136]
2f.	[Al, Teflon, Be]	[0.2151, 2.6260, 3.7330]
2g.	[Fe, Be]	[1.4035, 2.8271]
2h.	[Peth, Al, Air, Fe]	[1.7489, 2.4271, 3.0819, 3.6769]
2i.	[Air, Al, Teflon]	[0.8161, 1.8739, 2.0518, 3.7236]
2j.	[Be, Peth, Fe]	[1.3628, 1.9025, 3.6278]

rial attenuates the x-ray photons differently. For ease of calculation, the x-ray source spectrum was discretized because, for the materials examined, the attenuation at each of the energy levels is known. A single attenuation coefficient value for each material was calculated by taking the intensity-weighted average of the attenuations at each energy level. A second way to find $a(m)$ is to use the discretized energy levels of the x-ray source, but not average the attenuations at each energy level. Instead a vector of material coefficient values for each of the discretized is passed used in the objective function. For each object configuration, the objective function

$$f(\mu) = \frac{1}{L}\|P\mu - w^2 \ln(d)\|_2 \tag{4.1}$$

is evaluated to determine how well the current configuration matches the data in the radiograph where P is the discretized Abel transform matrix, d is the attenuation data from the radiograph, L is the size of the radiograph, and w is the radiograph pixel size. The variable μ is actually a function $\mu = \mu(n, x, a(m))$ of the number of material layers n, material edge locations x, and the attenuation coefficients (single or vector form) $a(m)$ of the material layers m.

4.3 Numerical Results

4.3.1 Object Test Set 1. In order to demonstrate the effectiveness of this implementation of the GPS algorithm with NOMADm [3], the algorithm was first tested on the object test set with the six combinations of Fe, Be, and Peth whose radiographs were generated using the single attenuation coefficient. To keep computational time down, the minimum and maximum number of allowable material layers were set to $n_{min} = 1$ and $n_{max} = 6$, respectively, and the minimum layer thickness was set at $\delta = 0.1$ cm. The initial guess which was a single layer of Fe with a thickness of 2.7 cm, was used because it is a reasonable representation of an unknown object.

GPS parameters were set as follows. The extended poll trigger was set at 0.99. At this value, extended polling occurred whenever a neighboring object's configuration resulted in an objective function value that was less than 99% higher than that of the current best configuration. The initial mesh size was set at 0.25 cm and doubled ($\tau = 2, w_k = 1$) whenever an improved mesh point was found. If not, the mesh size was divided in half ($w_k = -1$).

Table 4.5 shows the numerical results from NOMADm. The first column contains the object number from Table 4.3, while the second column contains the number of function values required to obtain an approximate solution. The third and fourth columns contain the material edge locations x and the material layer composition m, respectively. The fifth column contains the objective function values of each configuration, while the final column contains the objective function for the actual object composition from Table 4.3. Graphical representations of these object reconstructions can be found in Appendix A. Since it is bounded below by zero, the objective function value gives a numerical value for how well the object's composition matches the radiograph data. As column six demonstrates, even with the actual object, a perfect match to the radiograph data is not possible. This is due to the Poisson noise introduced into the radiograph simulation.

The GPS algorithm terminated when the mesh size dropped below the convergence tolerance of 0.001. This value was originally set at 0.02 to match the pixel size on the radiograph; however, we discovered that the objective function was highly sensitive to material edge

Table 4.5: Object Test Set 1, Single Attenuation Value Objective Function, Summation Radiographs.

Object	f Evals	$x(cm)$	m	f	Truth f
1a.	5588	[1.000, 1.997, 3.002]	[Fe, Be, Peth]	.018	.018
1b.	5046	[0.998, 1.999, 3.000]	[Fe, Peth, Be]	.020	.020
1c.	4492	[1.004, 2.001, 3.002]	[Be, Fe, Peth]	.026	.026
1d.	5331	[0.920, 2.000, 3.001]	[Be, Peth, Fe]	.039	.040
1e.	5686	[0.999, 1.999, 2.998]	[Peth, Fe, Be]	.028	.028
1f.	9813	[1.252, 1.244, 2.004, 2.991, 3.091]	[Peth, Teflon, Be, Fe, Peth]	.040	.037

location for this test set. For example, in Test Case 1b, if the algorithm tested the configuration $x = [.9801, 1.9801, 2.9801]$ and $m =$ [Fe, Peth, Be], the resulting objective function value would be 0.0370. The edge locations are all within .02 of the truth and the configuration $x = [1.000, 2.000, 3.000]$ would not be considered because the convergence tolerance was set at .02. Although no formal testing was performed on these parameters, higher extended poll trigger values or coarsening factors and lower convergence tolerances or refinement factors resulted in many more objective function evaluations.

As Table 4.5 shows, the algorithm successfully reconstructed five out of six of the test objects. Even though the algorithm was not able to accurately reconstruct test case 1f, it found another object whose configuration is also highly likely given the data. The actual object produced an objective function that was only .003 lower than that of the object found by GPS algorithm. A graphical representation of the case is displayed in Figure 4.1.

Figure 4.2 shows the graphical output from NOMADm for Test Case 1b. The number of function evaluations are plotted against the objective function value of the object the algorithm has found that most closely matches the radiograph data. It shows a rapid decrease of the objective function value early followed by a long plateau with limited improvement. This is consistent with observed behavior of derivative-free methods [37].

4.3.2 Object Test Set 2. With the success of the algorithm demonstrated on Object Test 1 and the GPS parameters of initial mesh size, mesh coarsening and refining factors, extended

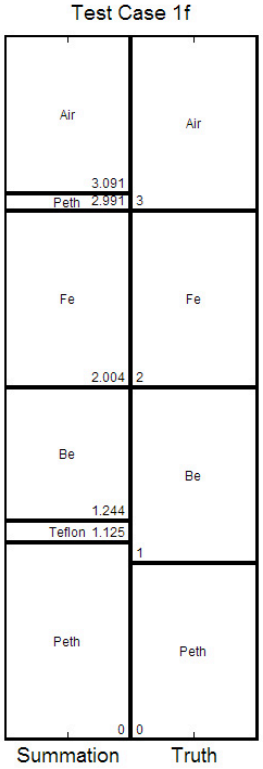

Figure 4.1: Graphical Representation Recreation of Test Case 1f

polling trigger values, and the convergence tolerance appropriately determined, the algorithm was then tested on Object Test Set 2 with these same parameters using the single averaged attenuation coefficient value for each of the materials. As Table 4.6 shows, the algorithm was only able to accurately reconstruct 4 out of the 10 objects. Graphical representations of these reconstructions can be found in Appendix A. Because of poor performance using the single attenuation coefficient for each material, Object Test Set 2 was tested using the vector of attenuation coefficients for each material.

The results for these runs are summarized in Table 4.7 and graphical representations are also found in Appendix A. Although these runs performed better than those using the single attenuation

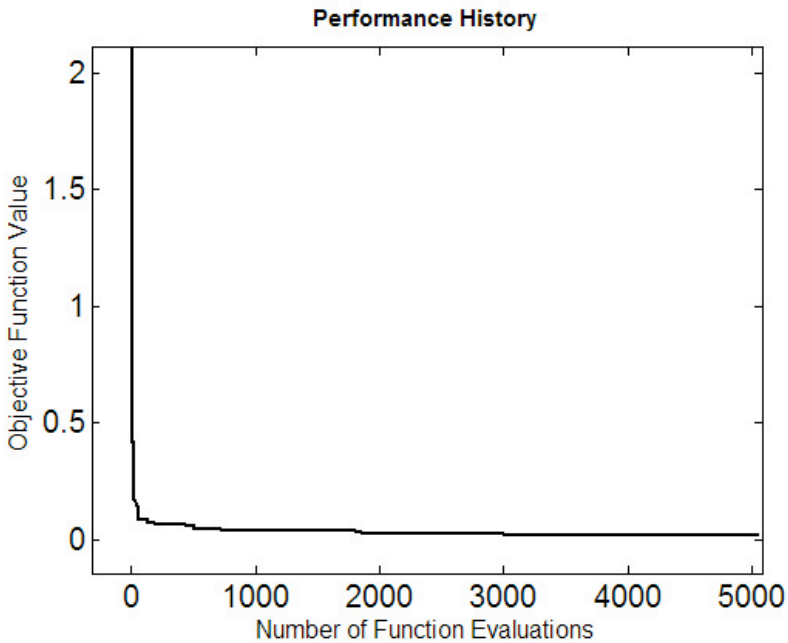

Figure 4.2: Output from NOMADm for Test Case 1b

coefficient, the algorithm was still only able to accurately reconstruct 5 out of the 10 objects in Object Test Set 2. However, the five failures show us a great deal about the behavior of the GPS algorithm on the LANL problem and avenues for improvement.

In test cases 2f and 2i using the vector of attenuation coefficients, GPS actually found a material configuration with a lower objective function value than that of the actual object, meaning that the configuration found numerically more closely matched the radiograph data than the actual object did. This is most likely the result of the natural occurring Poisson noise that is present in the x-ray radiograph process, and it shows that GPS can find incorrect object configurations due solely to this noise. The important point here is that the GPS algorithm actually performed as desired and reconstructed an object with the lowest objective function value.

In Test Cases 2a, 2h, and 2j, the incorrect configurations found were local approximate solutions, as defined by the choice of discrete neighbors. In each case, the number of material layers found was two less that the true number of layers because the discrete neighborhood function

Table 4.6: Object Test Set 2, Single Attenuation Value Objective Function, Summation Radiographs.

Object	f Evals	$x(cm)$	m	f	Truth f
2a.	306	[2.651]	[Fe]	.393	.046
2b.	441	[2.493]	[Be]	.008	.008
2c.	959	[1.713, 2.444]	[Be, Fe]	.014	.014
2d.	650	[3.432, 3.578, 3.700]	[Air, Peth, Al]	.075	.007
2e.	3333	[0.229, 0.084, 1.966, 3.413]	[Be, Air, Teflon, Be]	.008	.008
2f.	876	[2.631, 3.733]	[Teflon, Be]	.011	.010
2g.	2046	[1.403, 2.8273]	[Fe, Be]	.0140	.0140
2h.	1650	[3.899]	[Al]	.746	.017
2i.	537	[1.972, 3.271]	[Teflon, Al]	.107	.012
2j.	1869	[1.922, 3.626]	[Be, Fe]	.058	.043

Table 4.7: Object Test Set 2, Vector Attenuation Value Objective Function, MCNP No Scatter Radiographs.

Object	f Evals	$x(cm)$	m	f	Truth f
2a.	139	[2.672]	[Fe]	.210	.021
2b.	463	[2.493]	[Be]	.009	.010
2c.	959	[1.705, 2.442]	[Be, Fe]	.014	.014
2d.	475	[3.596, 3.800]	[Air, Al]	.016	.009
2e.	8873	[0.245, 0.850, 1.934, 3.413]	[Be, Air, Teflon, Be]	.011	.011
2f.	450	[2.573, 3.730]	[Teflon, Be]	.015	.018
2g.	1770	[1.406, 2.836]	[Fe, Be]	.0121	.0140
2h.	1650	[1.626, 3.137, 3.673]	[Peth, Be, Fe]	.114	.021
2i.	1268	[0.852, 3.719]	[Peth, Al]	.019	.047
2j.	3752	[0.399, 1.922, 3.627]	[Peth, Be, Fe]	.033	.026

only considers the addition of only layer at a time. As a result, adding one of the missing material layers produced a higher objective function value, and there was no opportunity to add the second missing material layer.

In addition to missing two material layers, Test Case 2a was also sensitive to the initial guess which was set to $x = [2.7]$ and $m =$ [Fe] for all cases. However, Test Case 2a was also tested with a initial (equivalent) guess of $x = [1.0, 2.0, 2.7]$ and $m =$ [Fe, Fe, Fe]. Although this initial guess has the same objective function value, the GPS algorithm was able to accurately reconstruct Test Case 2a in this case, because the algorithm started with the correct number (3) of materials. This case demonstrates that the solution space is relatively flat and consists of several local optima, and utilizing any prior knowledge of the object will be helpful. Finding the correct local optima was dependent of starting location. This is the result of the fact that, with Fe on the outermost material layer, materials interior have less of an effect on the attenuation. Further examination of this occurrence should be considered in future research.

4.3.3 Object Test Set 2 extensions. In all the previous test cases, the effects of scattering discussed in Chapter II were ignored in order to test the effectiveness of the GPS algorithm. An additional set of radiographs were generated that included the effects of scattering and the results of the algorithm using the vector of attenuation coefficients are found in Table 4.8. As comparison of the objective functions show, the algorithm found incorrect object configurations in 9 out of 10 cases that more closely matched the data than the actual object. This result is not surprising, but it verifies the need to correct for scattering prior to utilizing the GPS algorithm, either in the data or in the objective function.

In addition to testing cases that experience scattering, we also studied the case where the object x-rayed was larger in size than the radiograph. To avoid requiring new radiographs, this scenario was simulated by simply truncating the end of the radiograph data. This method was applied on Test Case 2e, using the vector attenuation value objective function with no scattering

Table 4.8: Object Test Set 2, Vector Attenuation Value Objective Function, MCNP Scattering Radiographs.

Object	f Evals	$x(cm)$	m	f	Truth f
2a.	3237	[1.310, 1.431, 1.553, 1.766, 2.706]	[Fe, Al, Be, Teflon, Be]	.081	.144
2b.	3273	[0.532, 0.634, 2.470]	[Be, Peth, Be]	.013	.018
2c.	4167	[1.504, 1.625, 1.730, 2.430]	[Be, Peth, Be, Fe]	.030	.053
2d.	358	[3.611, 3.799]	[Air, Al]	.014	.013
2e.	8563	[0.213, 0.871, 1.464, 3.268, 3.413]	[Be, Air, Teflon, Be, Peth]	.023	.061
2f.	2505	[1.234, 1.987, 3.696]	[Be, Teflon, Be]	.030	.289
2g.	2440	[1.368, 2.777]	[Fe, Be]	.047	.065
2h.	1004	[1.704, 3.800]	[Peth, Al]	.353	.118
2i.	1829	[0.910, 2.790]	[Peth, Teflon, Al]	.030	.098
2j.	1035	[2.127, 3.595]	[Be, Fe]	.144	.242

Table 4.9: Test Case 2e, Vector Attenuation Value Objective Function, MCNP No Scattering Radiographs at Different Sizes or Radiographs Used.

%	f Evals	$x(cm)$	m	f	Truth f
Full	8873	[0.245, 0.850, 1.934, 3.413]	[Be, Air, Teflon, Be]	.011	.011
95%	6034	[0.245, 0.850, 1.933, 3.415]	[Be, Air, Teflon, Be]	.011	.011
85%	8870	[0.243, 0.850, 1.929, 3.417]	[Be, Air, Teflon, Be]	.010	.011
75%	7229	[0.241, 0.852, 1.917, 3.425]	[Be, Air, Teflon, Be]	.010	.010
70%	19610	[0.241, 0.850, 1.042, 1.873, 2.905, 3.775]	[Be, Air, Be, Teflon, Be Peth]	.010	.010

considered. Table 4.9 shows the results of considering on a certain percentage (see Column 1) of the radiograph data while Figure 4.3 shows this graphically.

The algorithm was able to accurately reconstruct the object using only 75% of the radiograph data, but produced inaccurate reconstructions when using less data. The end of the radiograph contains information about the x-ray photons that passed through the transmission layer and the outermost material layer. It contains the most accurate data for the outermost material layer because some of the x-rays pass through only one material layer and do not experience complex attenuations due to passing through multiple layers as is seen near the center of the object.

In Test Case 2e, the outermost material layer occupied between 50% and 85% of the full radiograph. In this case, reducing the radiograph to 70% of its original size, which correlates to the

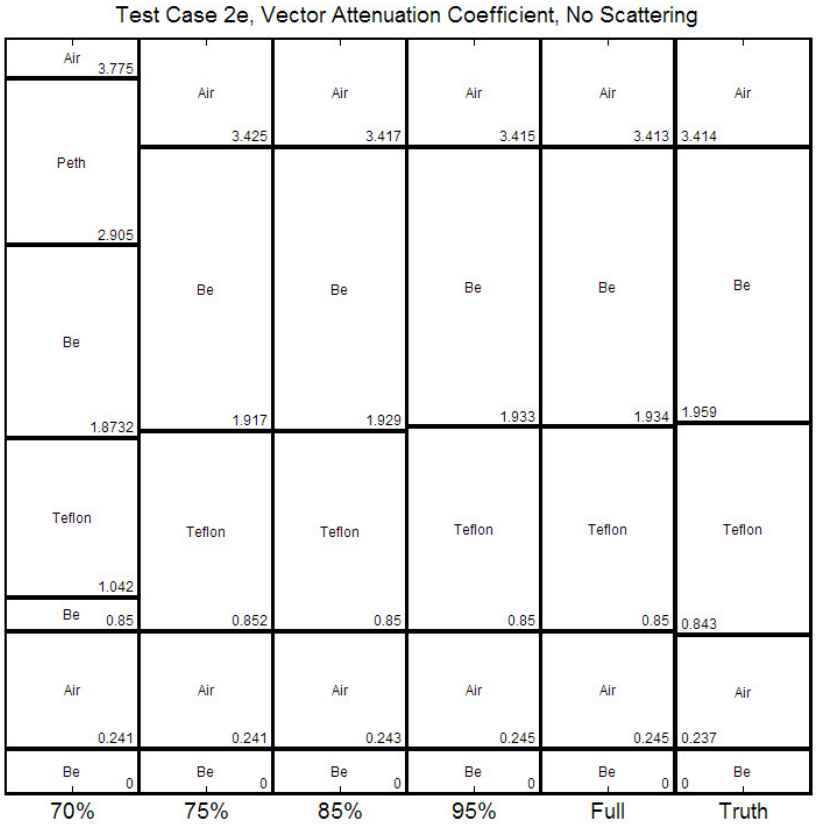

Figure 4.3: Graphical Representation of Test Case 2e at Different Radiograph Sizes

location of half the thickness of the outermost material layer, produced an incorrect reconstruction. Reducing the radiograph data below 75% removed valuable information about the outermost material that the algorithm needed in order to correctly identify the object's composition. As a result, this implies that GPS can be applied to objects that are smaller than the radiograph, but will begin to produce incorrect reconstructions if too much (in this case half) of the outermost material layer is not x-rayed.

In the next chapter, a summary of the research conclusions is provided. Additionally, further areas of research are identified as ways that may improve the accuracy of the GPS object reconstructions from x-ray radiographs of cylindrically symmetrical objects.

V. Conclusion

5.1 Research Conclusions

Quantitative reconstruction of cylindrically symmetrical objects normally requires LANL researchers an excessive amount of time to accomplish and fast methods (regularization) fail to produce a quantitative description. This work represents the first real success in this area, in which computational time is reasonable and the result is a quantitative description of the object. GPS is able to rapidly reconstruct an unknown object's composition from x-ray radiographs because of its ability to handle mixed variable problems and incorporate prior knowledge about the object. Although the GPS algorithm was not able to accurately construct the composition of all the objects, its success should not be judged solely on this fact. The algorithm only guarantees convergence to a local optimal point with respect to the discrete neighbors so the rules that govern the choices of the discrete neighbors will have a serious impact. Also, the initial guess chosen to test the algorithm was extremely poor. The methodology for solving the LANL problem shows promise. Better data, cost functions, discrete neighbor constructions and a more realistic initial guess will likely result in a more accurate reconstructions of an object.

The results from Chapter IV show that the algorithm generally finds an object whose composition closely matches the radiograph data. The closeness of the match is given by how low the objective function value is. A high objective function value is a clear indicator that the object composition found by the algorithm is most likely not the composition of the actual object. In some cases, the object reconstructed by the algorithm as a match to the radiograph data was not the same object that generated the data. In fact, using the vector of attenuation coefficients for each material in the objective function yielded some solutions that were better than the actual object, due to measurement noise. This represents a serious limitation to solving this type of problem if tight accuracy in object reconstruction is desired.

The failures of the GPS algorithm to reconstruct an object's composition actually provide more insight into the problem than the successful reconstructions. For example, in Test Set 2, the

single attenuation coefficient was found to be inadequate when trying to reconstruct objects that contained materials other than Peth, Be, and Fe. Additionally, the GPS algorithm will only solve the problem it is given. Testing with radiographs that included the effects of scattering shows that if the objective function does not accurately model the physical effects of the problem, the algorithm actually solves a different problem, whose solution may be quite different from the object that was x-rayed. Also, truncating the radiograph in Test Case 2e shows that the algorithm can find correct reconstructions from objects larger than the radiograph, but the accuracy of the reconstruction degrades, and will ultimately produce an incorrect reconstruction if not enough of the object is x-rayed.

5.2 Further Research

The reasons for the failure of the GPS algorithm to accurately reconstruct objects 2a, 2h, and 2j when using the vector of attenuation coefficients for each material supports the need to perform further research in several areas. The first involves the setting of the NOMADm parameters, specifically the extended poll trigger, the initial mesh size, the convergence tolerance, and the coarsening and refinement factors. Informal testing was performed on these parameters using objects from Test Set 1. The values were chosen in order to reduce the number of function evaluations required to accurately reconstruct the objects from Test Set 1. Formal design and analysis testing should be performed on these parameters with the objects in Test Set 2 to determine if they have an effect on the accuracy of the reconstruction of the objects and their effect on the number of function evaluations required.

In addition to parameter testing, the discrete neighborhood rules need to be examined. The rules for swapping, adding, and deleting a material layers were chosen in order to limit the number of function evaluations required. The fact that the object reconstructions often lacked two material layers suggests that a less restrictive rule for adding a material layer should be examined, perhaps one that allows for two layers of materials to be added at a time. This would result in a more global neighborhood structure and would require more function evaluations. To overcome the

computational cost of more function evaluations, a surrogate could be used to make the function evaluations cheaper. Also, the fact that the algorithm accurately reconstructed the composition of Test Case 2a when using a different starting point suggests that if the solutions space is indeed relatively flat and contains many local optima, a multi-point initial guess strategy may be effective. Also, incorporating any prior information about the object's composition, no matter how minor, could help the algorithm more accurately reconstruct objects.

Since the algorithm only guarantees convergence to a local minimizer, a meta-search heuristic, such as Tabu Search or Simulated Annealing, integrated into the GPS algorithm might prove to be effective at escaping local minima in the hopes of finding a better one, while preserving the convergence properties of the GPS algorithm. The GPS algorithm applied to the LANL problem has demonstrated to be a viable method for reconstructing cylindrically symmetrical objects from x-ray radiograph data and incorporating the results of further research will likely result in better solutions to these problems.

Appendix A. Graphical Representation of Test Results

The following figures give graphical representations for each object reconstruction in the test runs performed in Section 4.3. Pages A-2 and A-3 show the six Test Set 1 results using the single attenuation coefficient. In each case, the reconstructed object (Summation) is on the left, while the object that produced the x-ray radiograph (Truth) is on the right. Pages A-4 through A-13 show the Test Set 2 results. The x-rayed object (Truth) is on the far right, followed right-to-left by the reconstruction using the vector of attenuation coefficients from the radiographs with scattering (Scattering) and the scattering removed (No Scattering). The object reconstruction on the far left (Summation) is the one that used the single attenuation coefficient. The final figure shows the reconstruction of Test Case 2e using truncated radiographs. The percentages at the bottom of the figure indicate how much of the radiograph was used.

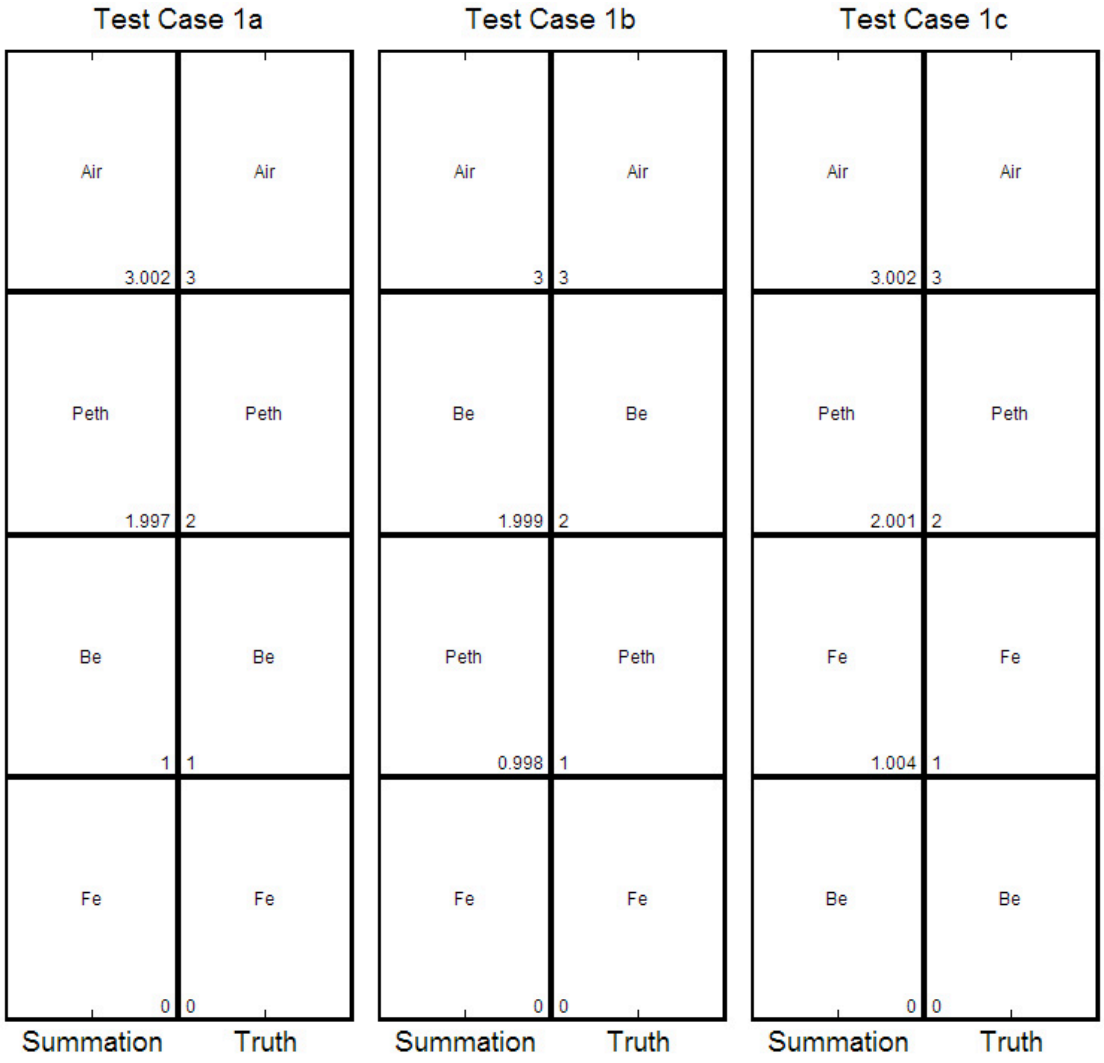
Test Case 1a
Air
Air
3.002
3
Peth
Peth
1.997
2
Be
Be
1
1
Fe
Fe
0
0
Summation
Truth
Test Case 1b
Air
Air
3
3
Be
Be
1.999
2
Peth
Peth
0.998
1
Fe
Fe
0
0
Summation
Truth
Test Case 1c
Air
Air
3.002
3
Peth
Peth
2.001
2
Fe
Fe
1.004
1
Be
Be
0
0
Summation
Truth

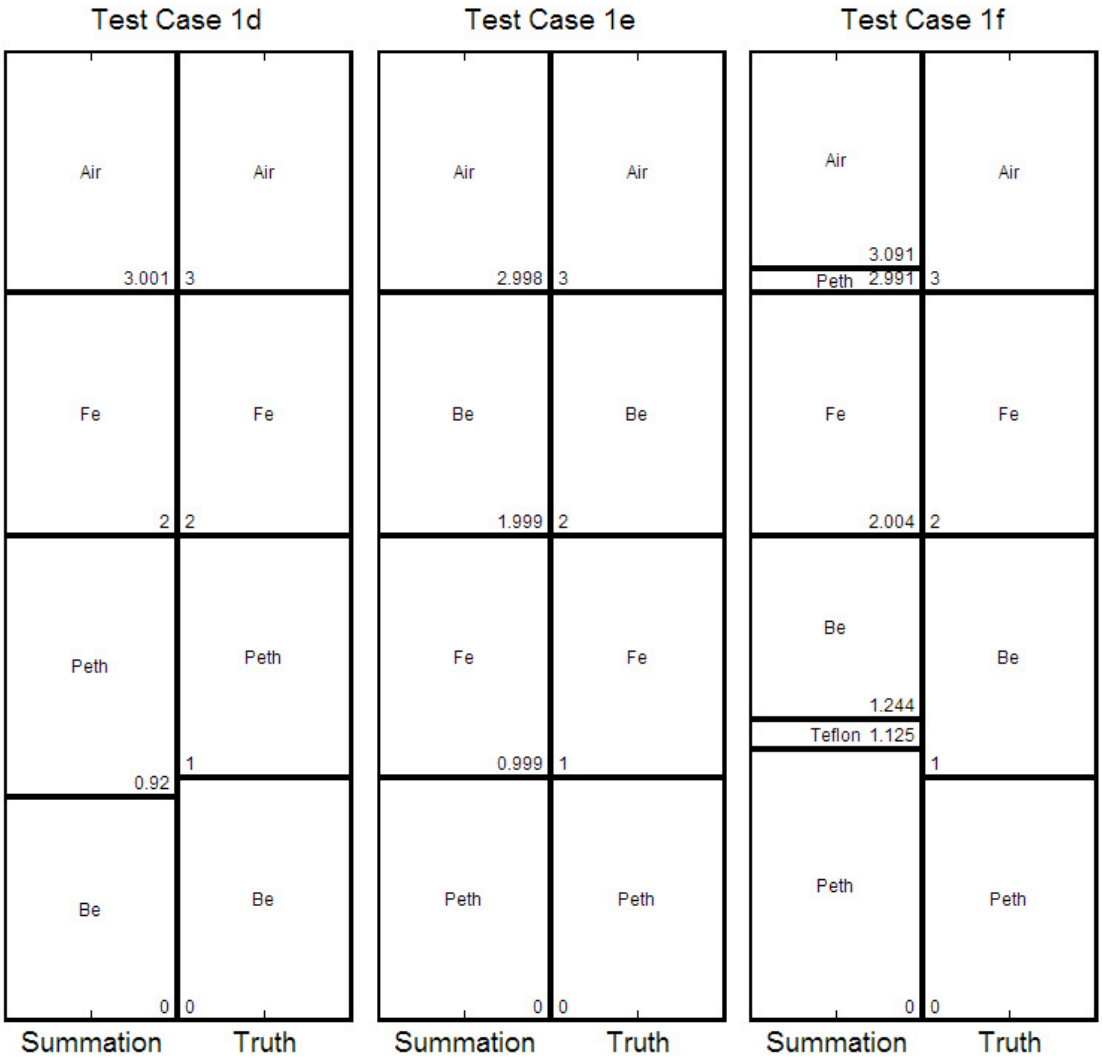
Test Case 1d
Air
Air
3.001
3
Fe
Fe
2
2
Peth
Peth
0.92
1
Be
Be
0
0
Summation
Truth
Test Case 1e
Air
Air
2.998
3
Be
Be
1.999
2
Fe
Fe
0.999
1
Peth
Peth
0
0
Summation
Truth
Test Case 1f
Air
Air
3.091
Peth 2.991
3
Fe
Fe
2.004
2
Be
Be
1.244
Teflon 1.125
1
Peth
Peth
0
0
Summation
Truth

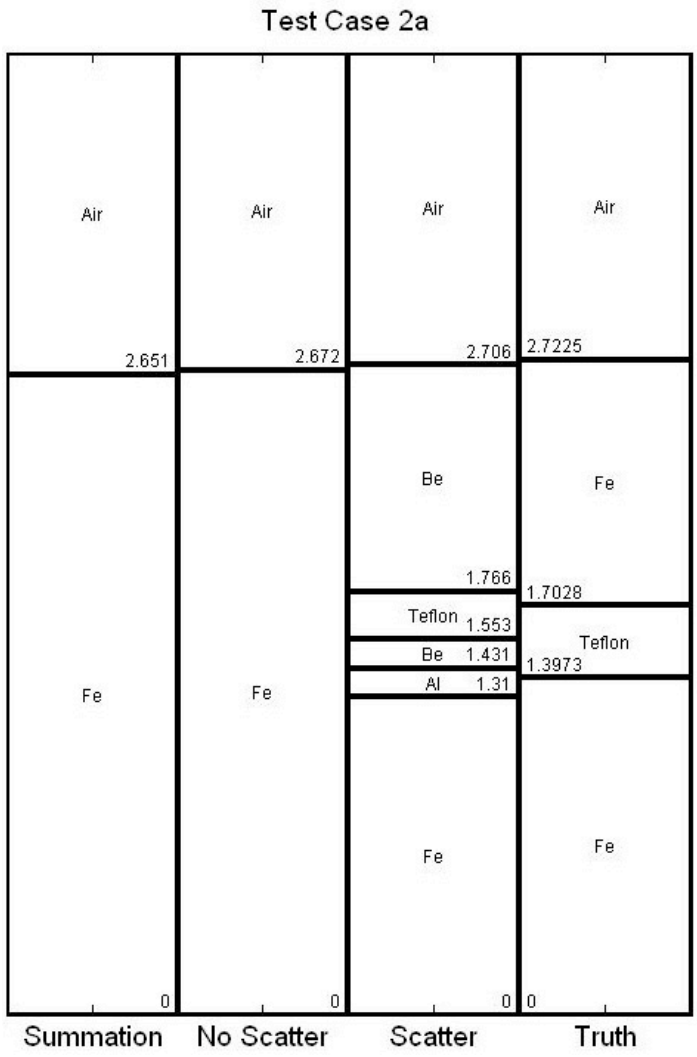
Test Case 2a
Air
2.651
Fe
0
Air
2.672
Fe
0
Air
2.706
Be
1.766
Teflon
1.553
Be
1.431
Al
1.31
Fe
0
Air
2.7225
Fe
1.7028
Teflon
1.3973
Fe
0
Summation
No Scatter
Scatter
Truth

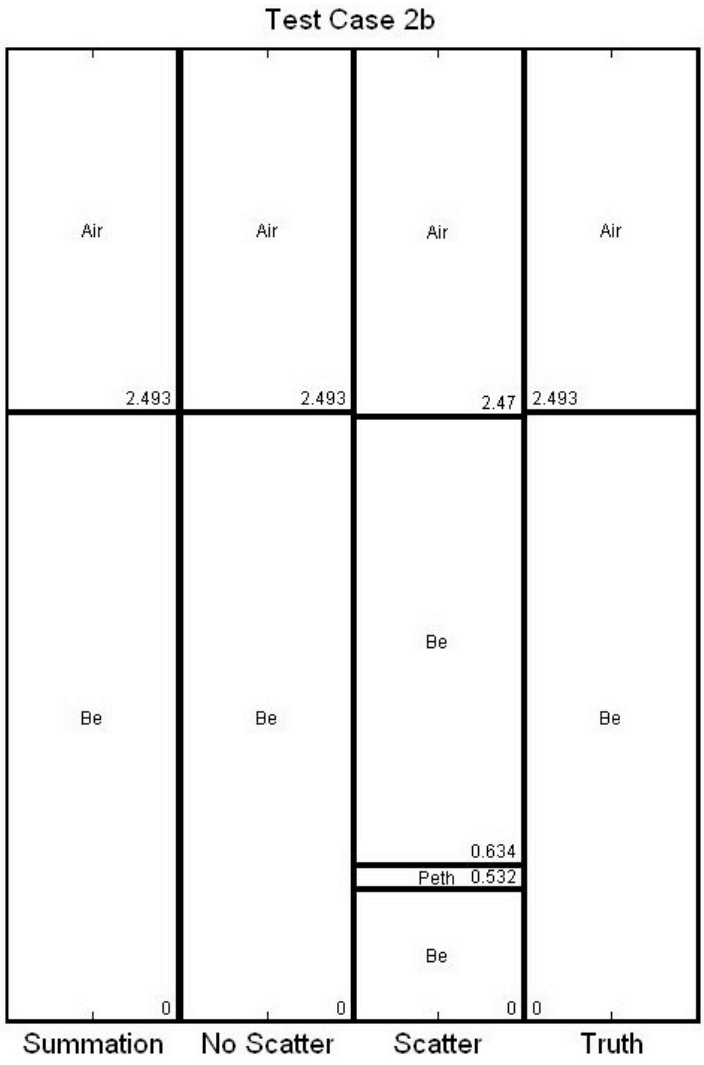
Test Case 2b
Air
2.493
Air
2.493
Air
2.47
Air
2.493
Be
0
Be
0
Be
0.634
Peth 0.532
Be
0
Be
0
Summation
No Scatter
Scatter
Truth

Test Case 2c

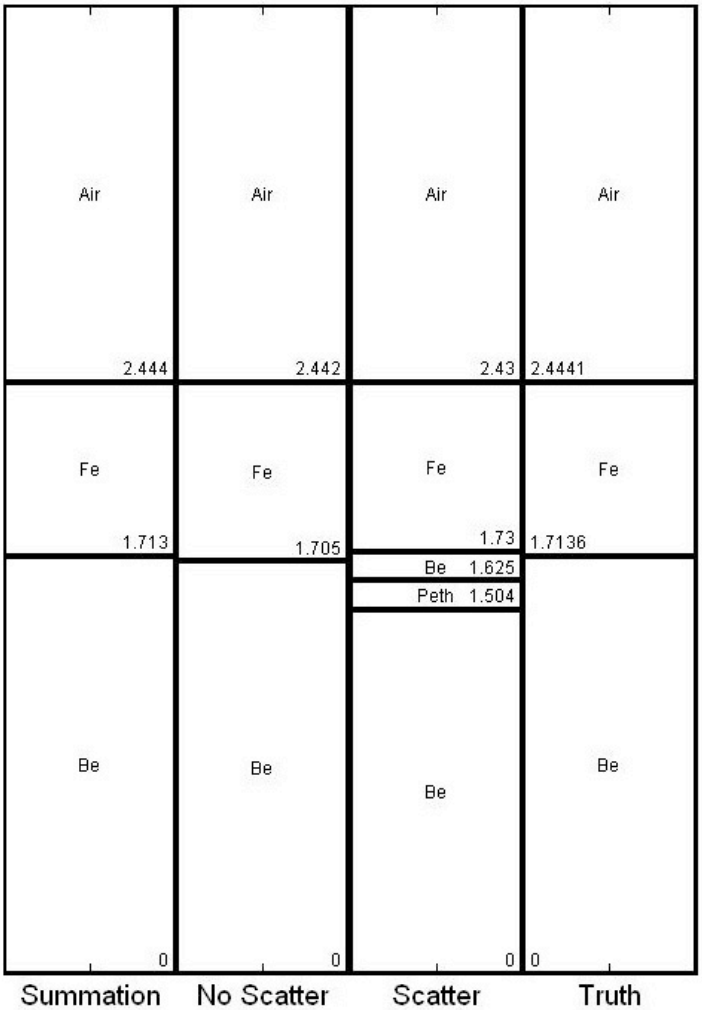
Air
2.444
Air
2.442
Air
2.43
Air
2.4441
Fe
1.713
Fe
1.705
Fe
1.73
Fe
1.7136
Be 1.625
Peth 1.504
Be
0
Be
0
Be
0
Be
0
Summation
No Scatter
Scatter
Truth

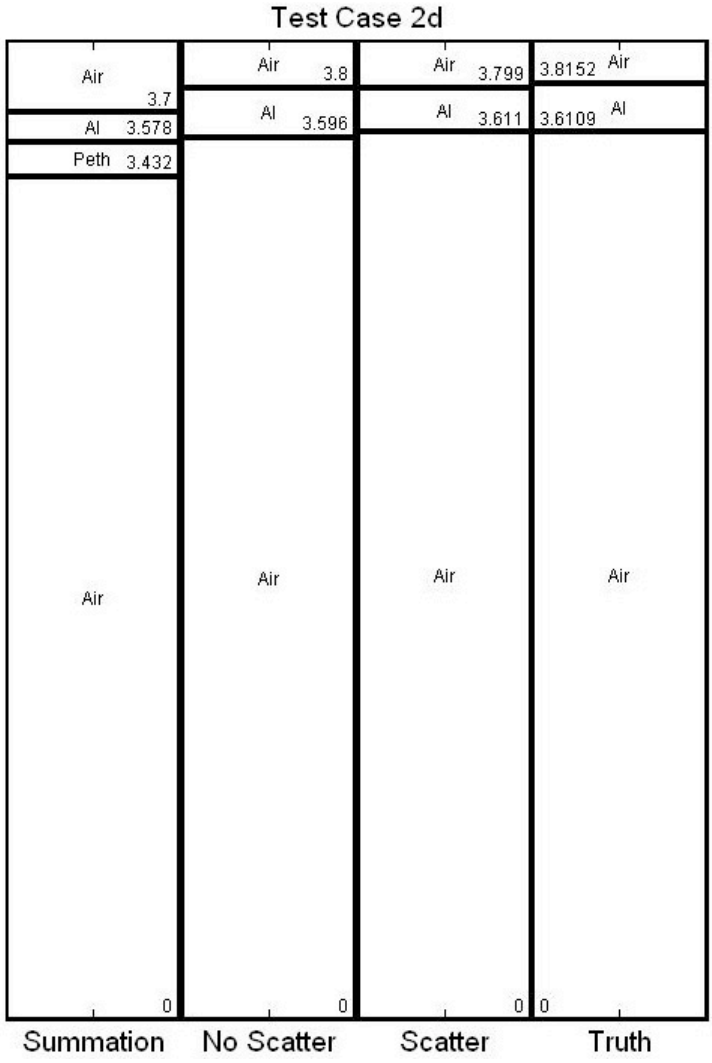
Test Case 2d
Air
3.7
Al
3.578
Peth
3.432
Air
0
Air
3.8
Al
3.596
Air
0
Air
3.799
Al
3.611
Air
0
3.8152
Air
Al
3.6109
Air
0
Summation
No Scatter
Scatter
Truth

Test Set 2e

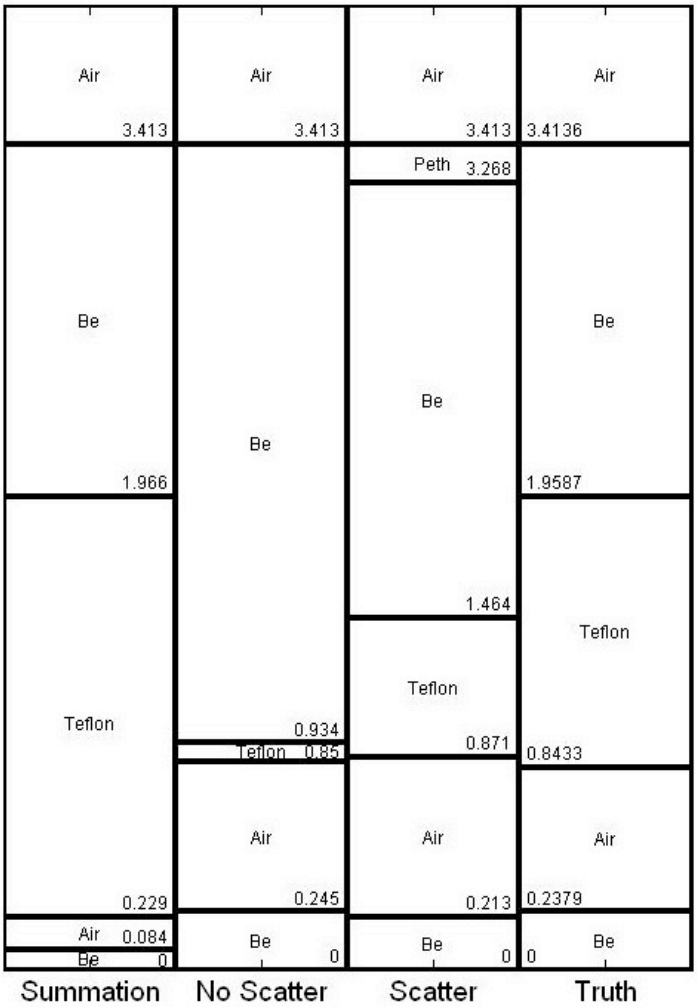
Air
3.413
Air
3.413
Air
3.413
Air
3.4136
Peth
3.268
Be
1.966
Be
Be
1.9587
1.464
Teflon
Teflon
0.934
Teflon
0.85
0.871
0.8433
Air
0.229
Air
0.245
Air
0.213
Air
0.2379
Air
0.084
Be
0
Be
0
Be
0
0
Be
Summation
No Scatter
Scatter
Truth

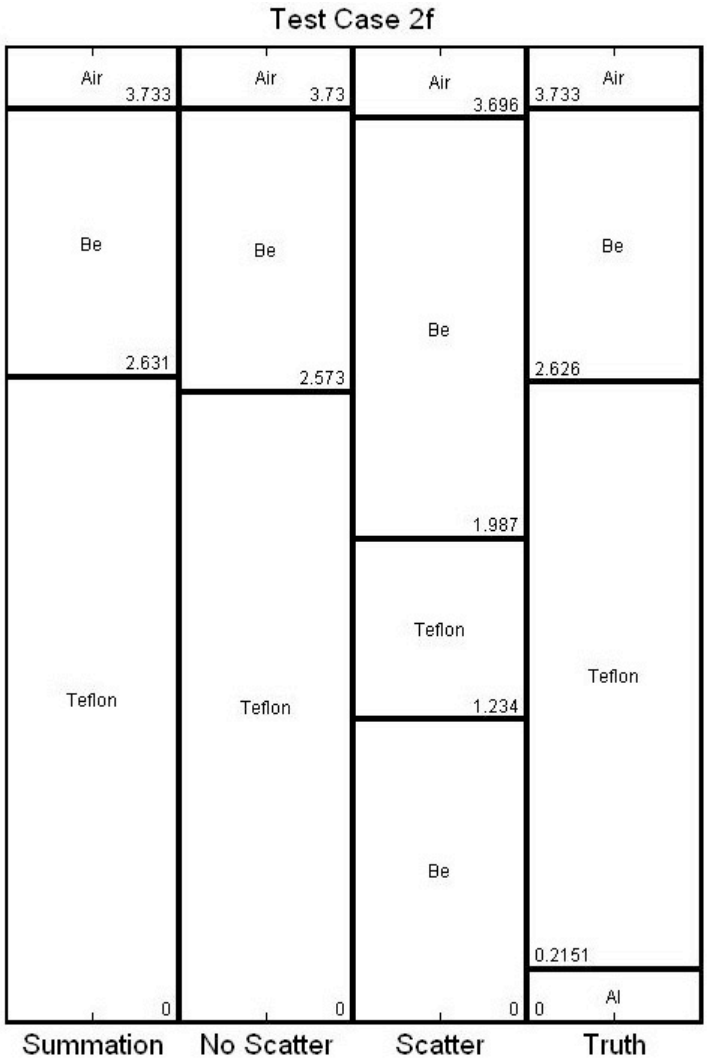
Test Case 2f
Air
3.733
Be
2.631
Teflon
0
Air
3.73
Be
2.573
Teflon
0
Air
3.696
Be
1.987
Teflon
1.234
Be
0
Air
3.733
Be
2.626
Teflon
0.2151
Al
0
Summation
No Scatter
Scatter
Truth

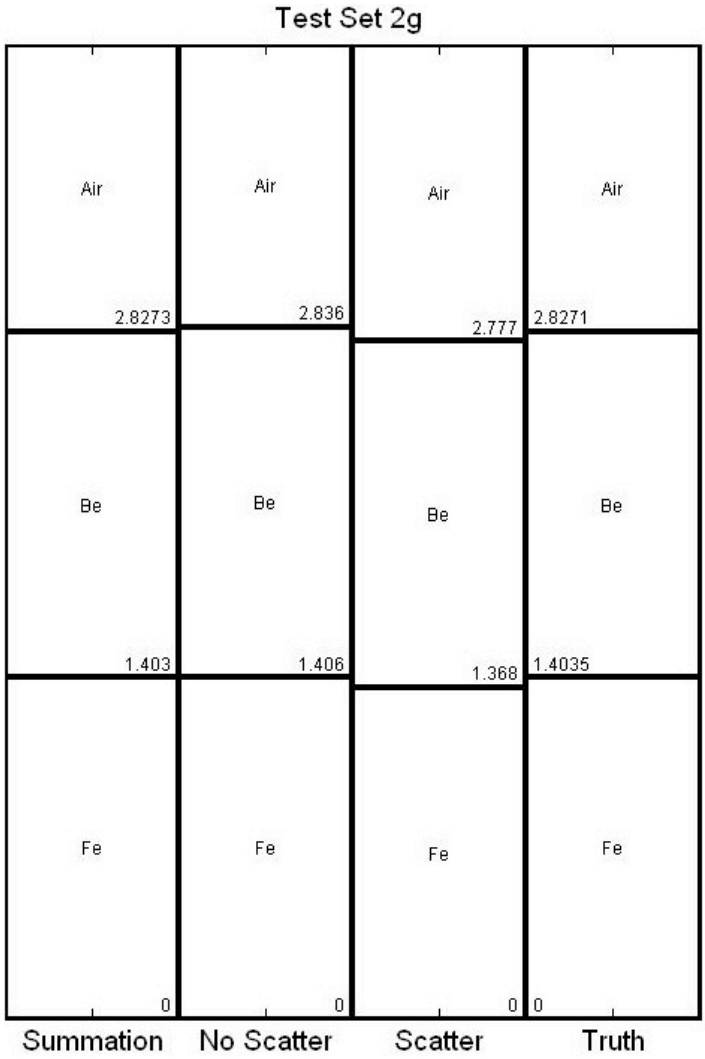
Test Set 2g
Air
2.8273
Air
2.836
Air
2.777
Air
2.8271
Be
1.403
Be
1.406
Be
1.368
Be
1.4035
Fe
0
Fe
0
Fe
0
Fe
0
Summation
No Scatter
Scatter
Truth

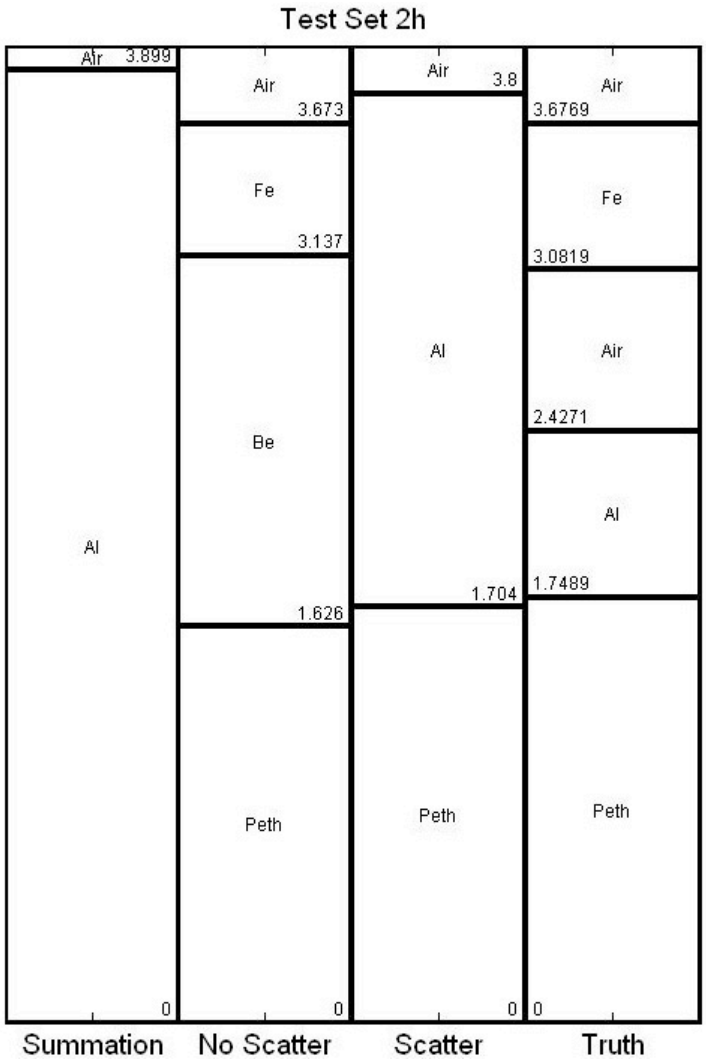
Test Set 2h
Air
3.899
Al
0
Air
3.673
Fe
3.137
Be
1.626
Peth
0
Air
3.8
Al
1.704
Peth
0
Air
3.6769
Fe
3.0819
Air
2.4271
Al
1.7489
Peth
0
Summation
No Scatter
Scatter
Truth

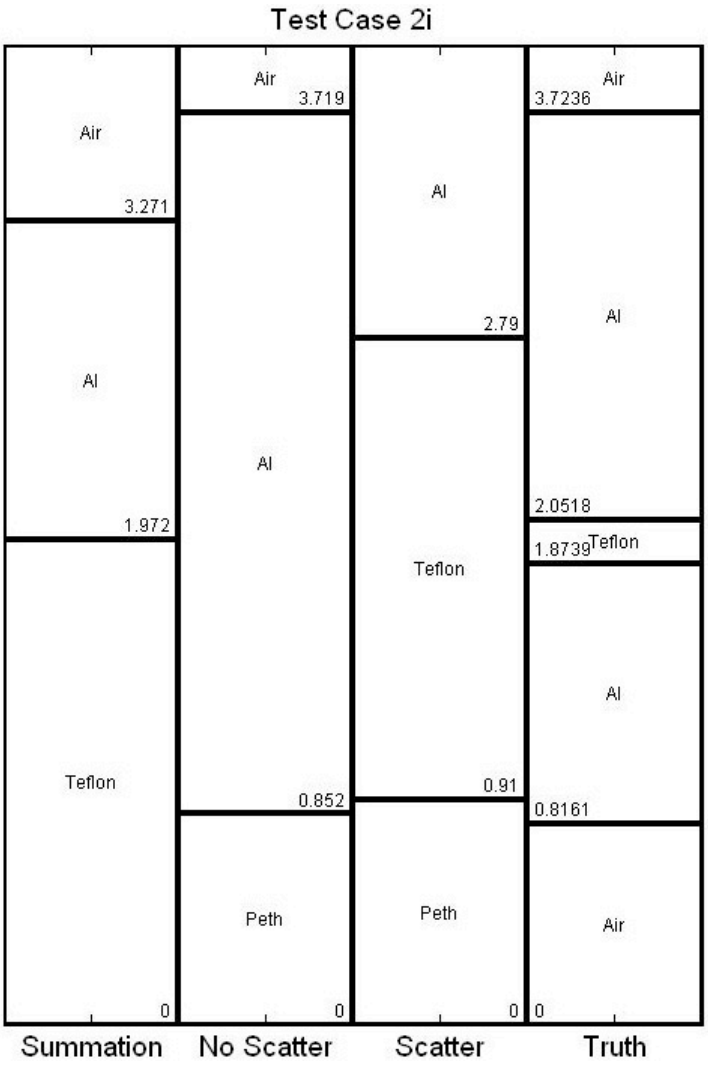
Test Case 2i
Air
3.271
Al
1.972
Teflon
0
Air
3.719
Al
0.852
Peth
0
Al
2.79
Teflon
0.91
Peth
0
Air
3.7236
Al
2.0518
Teflon
1.8739
Al
0.8161
Air
0
Summation
No Scatter
Scatter
Truth

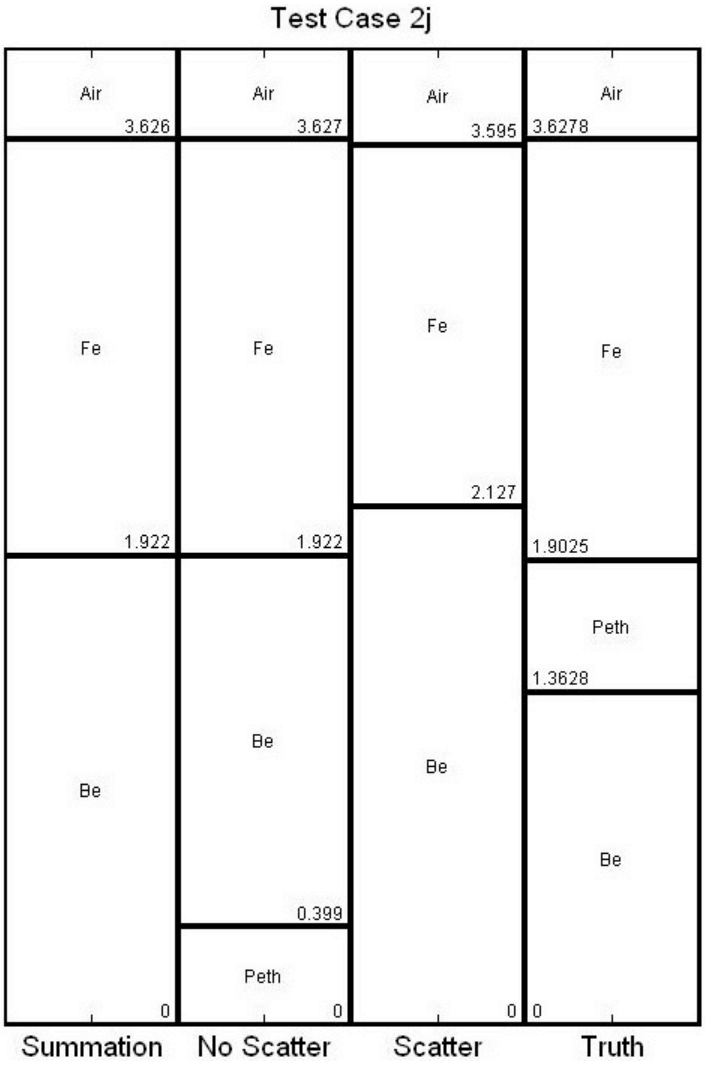
Test Case 2j
Air
3.626
Fe
1.922
Be
0
Air
3.627
Fe
1.922
Be
0.399
Peth
0
Air
3.595
Fe
2.127
Be
0
Air
3.6278
Fe
1.9025
Peth
1.3628
Be
0
Summation
No Scatter
Scatter
Truth

Test Case 2e, Vector Attenuation Coefficient, No Scattering

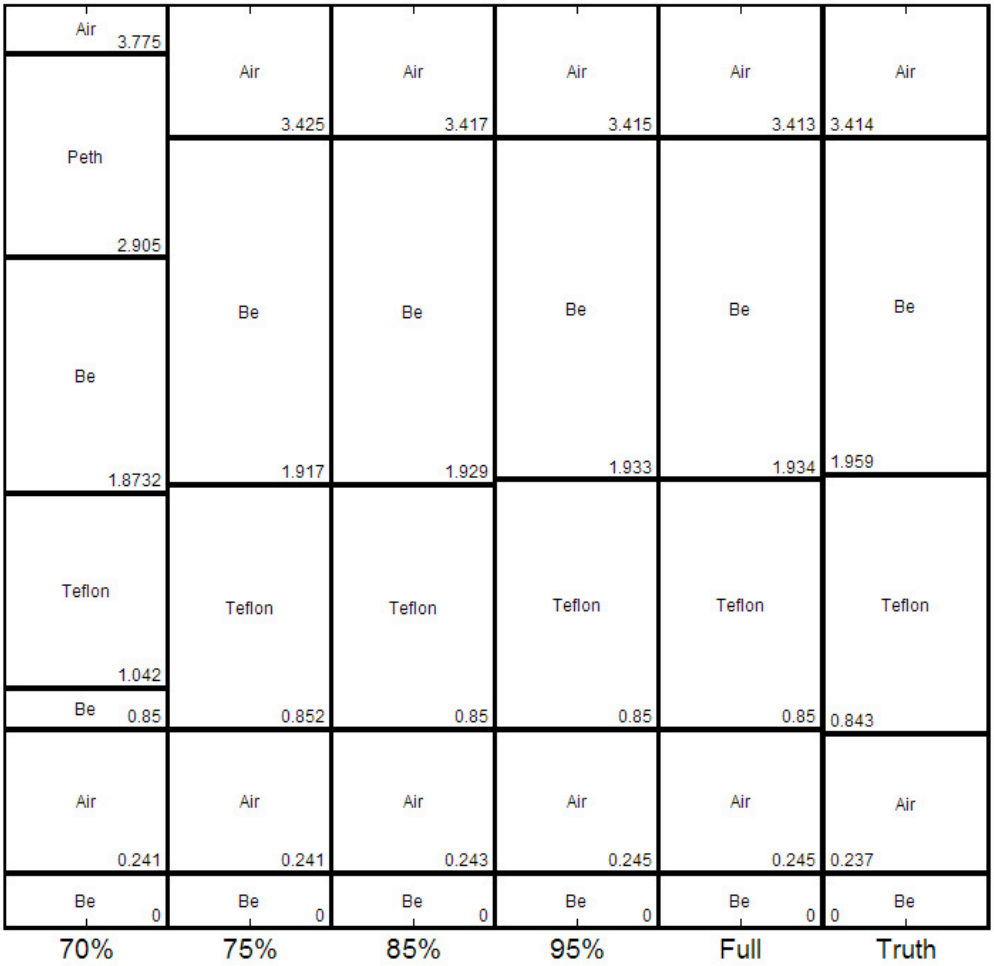

Appendix B. MATLAB® Code

The following contains the MATLAB® code used to implement the GPS algorithm on LANL reconstruction problem. The first five files are required by the NOMADm software, while the last two implement the objective function using the single attenuation coefficient and the vector of attenuation coefficients, respectively, for each material.

B.1 Main Function File

```
%*************************************************************************
% x_ray:  Computes the objective function value for the X-Ray mixed
%         variable optimization problem
% -------------------------------------------------------------------------
% Variables:
%   cx                      = unused
%   fx                      = objective function value
%   x                       = layer edge locations (continuous variables)
%   p                       = layer materials (catgorical variables)
%   material                = layer materials (polychromatic numerical
%                             values)
%   n                       = number of layers
%   Param                   = structure containing all paramaters for the
%                             optimization problem
%       .C                  = continuous case flag
%       .cost               = cost function being used
%       .EndEdgeLocation    = location of outer edge of last layer
%       .EndEdgeMaterial    = material of last layer (usually air)
%       .Materials          = array of possible material
%       .mu                 = array of attenuation coefficients for
%                             possible materials
%       .Q                  = Discrete Abel Matrix, data, and coefficient
%*************************************************************************

function [fx,cx] = x_ray(x,p);

Param = getappdata(0,'PARAM');
n=p{1};

% Set up Cost Function for Continous Case
if Param.C==1;
    %  Add back removed layer of outer edge material
    material = [x(n+1:end); Param.EndEdgeMaterial];
    x=[x(1:n); Param.EndEdgeLocation];

% Set up Cost Function for Discrete Case
else
```

```
    material=[];
    p(1)=[];
    for k=1:n
        value=p(k);
        index=strmatch(value,Param.Materials,'exact');
        material = [material; Param.mu(index)];
    end

    %  Add back removed layer of outer edge material
    material=[material; Param.mu(strmatch(Param.EndEdgeMaterial,...
        Param.Materials,'exact'))];
    x=[x; Param.EndEdgeLocation];
end

% Increase number of layers to account for adding back removed outer layer
n=n+1;
fx = feval(Param.cost,n,x,material, Param.Q)
cx = [];

return
```

B.2 Parameter File

```
%*************************************************************************
% x_ray_Param:  Storage of global data for the optimization problem.
% -------------------------------------------------------------------------
% Variables:
%   Materials           = cell array of all possible materials that can
%                         be used
%   MaterialIndex       = vector of indices of Materials that will be used
%                         in the run
%   Param               = structure of optimization problem data
%     .Materials        = cell array list of possible layer material
%                         property values for this run
%     .MaxNumLayers     = maximum number of layers allowed
%     .MinNumLayers     = minimum number of layers allowed
%     .MinLayerWidth    = minimum width of each layer
%     .P_Min            = minimum value for x_ray return
%     .P_Max            = maximum value for x_ray return
%     .L                = radiograph size
%     .C                = continuous case flag
%     .EndEdgeLocation  = location of outer edge of last layer
%     .Materials        = array of possible materials
%     .MaxNumLayers     = maximum number of layers
%     .MinLayerWidth    = minimum layer width constraint
%     .MinNumLayers     = minimum number of layers
%     .P_max            = maximum attenuation value, used in continuous
%                         case only
%     .P_min            = minimum attenuation value, used in continuous
```

```
%                          case only
%*************************************************************************

function Param = x_ray_Param(varargin);

%  Continous? O for Discrete, 1 for Continous
Param.C=0;

% Choose Test Set
load('F:\Nomadm\xray\Test Sets\Discrete Set1\test_012_2_syn321.mat');

%Choose Cost Function
Param.cost='cost_002_linatt';

% Choose allowable materials by changing Library
load('F:\Nomadm\xray\Libraries\library_2_1_cyg002.mat');
%Param.energy=library.energy;

% Adjust for incorrect Data Set
%guess.edges=guess.edges*.02;

% Load Global Parameters
Param.EndEdgeLocation           =guess.edges(end);
Param.L                         =Param.EndEdgeLocation;
Param.Q                         =Q;
Param.Materials                 =library.names;
Param.mu                        =library.mu;
Param.Z                         =library.Z;
Param.Neighbors                 =N;
Param.InitialGuessEdges         =guess.edges(1:end-1);
for k=1:length(guess.edges)-1
   if Param.C
        Param.InitialGuessMaterial(k)=guess.materials(k);
        Param.EndEdgeMaterial=guess.materials(end);
   else
        Param.InitialGuessMaterial{k}=guess.materials{k};
        Param.EndEdgeMaterial=guess.materials{end};
    end
end
Param.NumMaterials  = length(Param.Neighbors);
Param.MinNumLayers  = constraint.minedges-1;
Param.MaxNumLayers  = constraint.maxedges-1;
Param.MinLayerWidth = constraint.minwidth;
% Continuous Case Additional Variables Required, not inputed
Param.P_min         = 0;
Param.P_max         = 4;

% Maximum problem dimensions
if Param.C
   Param.maxNp = 1;
```

```
   Param.maxNx = 2*Param.MaxNumLayers;
else
   Param.maxNp = Param.MaxNumLayers;
   Param.maxNx = Param.MaxNumLayers;
end

%  Allow for different initial parameters (Debugging only)!
Param.InitialGuessMaterial = {'Fe'};
Param.InitialGuessEdges=[2.7];

return
```

B.3 Initial Iterate File

```
%*************************************************************************
% x_ray_x0:  Contains the initial guess information for the X-Ray mixed
%            variable optimization problem
% -----------------------------------------------------------------------
% Variables:
%   iterate                     = structure of current iterate data
%       .x                      = current iterate layer edge locations
%                                 (continuous variables)
%       .p                      = current iterate layer materials
%                                 (catgorical variables)
%   Param                       = structure containing all paramaters for
%                                 the optimization
%       .C                      = continuous case flag
%       .InitialGuessEdges      = layer edge locations initial guess
%       .InitialGuessMaterial   = layer material initial guess
%*************************************************************************

function iterate = x_ray_x0

Param = getappdata(0,'PARAM');

% Original Starting Point Continous Case
if Param.C==1
    iterate.x = [Param.InitialGuessEdges'; Param.InitialGuessMaterial'];
    iterate.p{1}=length(Param.InitialGuessEdges);
else

    % Original starting point Discrete Case
    iterate.x = [Param.InitialGuessEdges'];
    iterate.p{1}=length(Param.InitialGuessEdges);
    for k=1:length(Param.InitialGuessEdges);
        iterate.p{k+1} = Param.InitialGuessMaterial{k};
    end
end
```

```
return
```

B.4 Linear Constraints File

```
%*********************************************************************
% x_ray_Omega:  Linear Constraints file for the problem, 'x_ray'.
% -------------------------------------------------------------------
% Variables:
%   A                       = linear constraint matrix
%   l                       = lower bound on linear constraints
%   u                       = upper bound on linear contraints
%   p                       = layer materials (catgorical variables)
%   n                       = number of layers
%   nx                      = unused
%   Param                   = structure containing all paramaters for
%                             the optimization problem
%       .C                  = continuous case flag
%       .EndEdgeLocation    = location of outer edge of last layer
%       .Materials          = array of possible materials
%       .MaxNumLayers       = maximum number of layers
%       .MinLayerWidth      = minimum layer width constraint
%       .MinNumLayers       = minimum number of layers
%       P_max               = maximum attenuation value, used in
%                             continuous case only
%       P_min               = minimum attenuation value, used in
%                           continuous case only
%    plist                  = cell array of possible p values: p{i}{j},
%                             i = variable, j =list
%*********************************************************************

function [A,l,u,plist] = x_ray_Omega(nx,p)

Param = getappdata(0,'PARAM');

% Develop list of possible categorical variable values
n = p{1};
plist{1} = {Param.MinNumLayers:Param.MaxNumLayers};

% Linear Constraints

%Continuous Case
if Param.C==1
   A = [eye(n)-diag(ones(n-1,1),-1), zeros(n);
       zeros(n), eye(n)];
   l = [ones(n,1)*Param.MinLayerWidth; ones(n,1)*Param.P_min];
   u = [ones(n,1)*(Param.EndEdgeLocation-Param.MinLayerWidth*(n)); ...
       ones(n,1)*Param.P_max];

% Discrete Case
```

```
else
   A = [eye(n)-diag(ones(n-1,1),-1); zeros(1,n-1), 1];
   l = [ones(n,1)*Param.MinLayerWidth; n*Param.MinLayerWidth];
   u = [ones(n,1)*(Param.EndEdgeLocation-Param.MinLayerWidth*(n));...
       Param.EndEdgeLocation-n*Param.MinLayerWidth];
   [plist{2:n+1}] = deal(Param.Materials);
end

return
```

B.5 Neighborhood Definition File

```
%*************************************************************************
% x_ray_N:  User-supplied function defining set of neighbors for a
%                a given vector of categorical variables p.
% -----------------------------------------------------------------------
%   Variables:
%     add                   = addition of layer flag
%     delete                = deletion of layer flag
%     delta                 = unused
%     index                 = adjacentcy matrix index of material being
%                             considered
%     innerindex            = adjacentcy matrix index of material layer to
%                             the inside of current layer considered
%     iterate               = current iterate for whom discrete neighbor
%                             point will be found.
%       .p                  = current iterate layer materials (catgorical
%                             variables)
%       .x                  = current iterate layer edge locations(continuo
%                             us variables)
%     neighbor              = iterate who is a neighbor of p
%       .p                  = layer materials of iterate who is a neighbor
%                             of p
%       .x                  = layer edge location of iterate who is a
%                             neighbor of p
%     N                     = vector of iterates who are neighbors of p
%     NumLayers             = number of layers in current iterate
%     outerindex            = adjacentcy matrix index of material layer to
%                             the outside of current layer considered
%     outerlayerindex       = adjacentcy matrix index of outside layer
%                             material (usually 1)
%     p                     = temporary iterate layer materials, used for
%                             calculations
%     Param                 = structure containing all paramaters for the
%                             optimization
%       .C                  = continuous case flag
%       .Materials          = array of possible materials
%       .MaxNumLayers       = maximum number of layers allowed
%       .MinNumLayers       = minimum number of layers
```

```
%       .P_max              = maximum attenuation value, used in continuous
%                             case only
%       .P_min              = minimum attenuation value, used in continuous
%                             case only
%     plist                 = cell array of possible p values: p{i}{j},
%                             i = variable, j = list
%     Problem               = unused
%     x                     = temporary layer edge locations used for
%                             calculation
%     y                     = temporary value used in calculations
%
%*************************************************************************

function N = x_ray_N(Problem,iterate,plist,delta);

Param = getappdata(0,'PARAM');
NumLayers = iterate.p{1};
N= [];
outerlayerindex=strmatch(Param.EndEdgeMaterial,Param.Materials,'exact');

%  Neighbor Definition for the Continous Case
if Param.C==1

    % Include neighbors in which a Layer is added
    if (NumLayers < Param.MaxNumLayers)
        x=iterate.x;

        % Determine value of added layers
        if x(1) <= Param.P_max/2
            x=[0;x(1:NumLayers); Param.P_min; x(NumLayers+1:end)];
        else
            x=[0;x(1:NumLayers); Param.P_max; x(NumLayers+1:end)];
        end

        % Calculate adjacent layer averages
        y=[(x(2:NumLayers+1)+x(1:NumLayers))/2; (x(NumLayers+3:end)+...
            x(NumLayers+2:end-1))/2];

        % Insert Added Layers
        for k = NumLayers:-1:1
            x=iterate.x;
            x=[x(1:k-1); y(k); x(k:NumLayers); x(NumLayers+1:...
                NumLayers+k-1); y(NumLayers+k); x(NumLayers+k:end)];
            neighbor.x = x;
            neighbor.p = iterate.p;
            neighbor.p{1} = NumLayers + 1;
            N = [N neighbor];
        end
    end
```

```
    % Include neighbors in which one edge is removed
    if (NumLayers > Param.MinNumLayers)
        for k = NumLayers:-1:1
            x=iterate.x;
            x(NumLayers+k)=[(iterate.x(NumLayers+k)+iterate.x(NumLayers+...
                (k+1)))/2];
            x(NumLayers+k+1)=[];
            x(k)=[];
            neighbor.x = x;
            neighbor.p = iterate.p;
            neighbor.p{1} = NumLayers - 1;
            N = [N neighbor];
        end
    end

% Neighbor Definitions for the Discrete Case
else

    % Include neighbors in which one material layer is removed
    if NumLayers > Param.MinNumLayers
        for k = NumLayers:-1:1
            p=iterate.p;
            delete=0;
            p(1)=[];
            index=strmatch(p(k),Param.Materials,'exact');

            % Case if outermost layer
            if k==NumLayers
                innerindex=strmatch(p(k-1),Param.Materials,'exact');
                if (Param.Neighbors(index, innerindex)==1 && innerindex=...
                        =outerlayerindex)
                    if NumLayers > 2
                        delete=2;
                    end
                elseif (Param.Neighbors(index, innerindex)==1 | ...
                        Param.Neighbors(index, outerlayerindex)==1)
                    delete=1;
                end

            % Case if inner most layer
            elseif k==1
                outerindex=strmatch(p(k+1),Param.Materials,'exact');
                if Param.Neighbors(index, outerindex)==1
                    delete=1;
                end

            % Other cases
            else
              innerindex=strmatch(p(k-1),Param.Materials,'exact');
              outerindex=strmatch(p(k+1),Param.Materials,'exact');
```

```
          if Param.Neighbors(index, outerindex)==1 | Param.Neighbors...
                  (index, innerindex)==1
                delete=1;
          end
        end

        %  Delete a layer
        if delete==1
                x=iterate.x;
                x(k)=[];
                neighbor.x=x;
                neighbor.p = iterate.p;
                neighbor.p{1} = NumLayers - 1;
                neighbor.p(k+1) = [];
                N = [N neighbor];
        elseif delete==2
                x=iterate.x;
                x(k-1:k)=[];
                neighbor.x=x;
                neighbor.p=iterate.p;
                neighbor.p{1}=NumLayers - 2;
                neighbor.p(k:k+1)=[];
                N= [N neighbor];
        end
    end
end

% Include neighbors in which 1 material layer is swaped
    for k = NumLayers:-1:1
        x=iterate.x;
        p=iterate.p;
        p(1)=[];
        index=strmatch(p(k),Param.Materials,'exact');
        % Check all materials
        for i=1:Param.NumMaterials
            %Prevent outermost layer from being duplicated
            if (~(k==NumLayers) | ~(i==outerlayerindex))
                if Param.Neighbors(index, i)==1
                    neighbor.x = iterate.x;
                    neighbor.p = iterate.p;
                    neighbor.p{k+1} = Param.Materials{i};
                    N = [N neighbor];
                end
            end
        end
    end

%  Include neighbors in which 1 material layer is added
if NumLayers < Param.MaxNumLayers
```

```
% Calculate adjacent layer averages
x=iterate.x;
p=iterate.p;
x=[0;x(1:NumLayers);Param.EndEdgeLocation];
y=[(x(2:NumLayers+2)+x(1:NumLayers+1))/2];

% Check for all layers
for k = NumLayers+1:-1:1
    x=iterate.x;
    p=iterate.p;
    x=[x(1:k-1);y(k);x(k:NumLayers)];
    % Check all materials
    for i=1:Param.NumMaterials
        add=0;

        % Outermost Layer case
        if k==NumLayers+1
            innerindex=strmatch(p(k),Param.Materials,'exact');
            if (Param.Neighbors(i, innerindex)==1 | ...
                    Param.Neighbors(i, outerlayerindex)==1)
                add=1;
            end

        % Innermost Layer case
        elseif k==1
            outerindex=strmatch(p(k+1),Param.Materials,'exact');
            if Param.Neighbors(i, outerindex)==1
                add=1;
            end

        % Other cases
        else
            innerindex=strmatch(p(k),Param.Materials,'exact');
            outerindex=strmatch(p(k+1),Param.Materials,'exact');
            if Param.Neighbors(i, outerindex)==1 | ...
                    Param.Neighbors(i, innerindex)==1
                add=1;
            end
        end

        % Add a layer
        if add==1;
            neighbor.x = x;
            neighbor.p = iterate.p;
            neighbor.p={NumLayers+1, iterate.p{2:k}, ...
                Param.Materials{i}, iterate.p{k+1:end}};
            N = [N neighbor];
        end
    end
end
```

```
    end
end

return
```

B.6 Objective Function 1 File

```
%*************************************************************************
% cost_002_linatt is a cost functional evaluation for
% use with the mixed-variable optimization X-ray inversion
% project.  It assumes an attenuation reconstruction
% from normalized transmission data. The norm assumes
% Guassian additive noise.
%
% This function differs from cost_001_linatt only in the
% last line -- here we use a data fidelity norm on the
% logarithm of the data
%
% USAGE:
% [cost] = cost_002_linatt(n,e,p,Q)
%
% INPUTS:
%   [The inputs constitute an object description]
% Q{1} = P is the Abel projection operator scaled to
%      unit data pixel size
% Q{2} = data is the vector of transmission data values
%      ordered from inside outward.  Values are assumed
%      to be normalized to unity for zero attenuation.
% Q{3} = w is the pixel width (and height) on the
%      detector in real units.
% n is the integer number of edges in the object
%   The edge of the data is included as an edge location.
% e is a vector of ring edge locations ordered from
%   inside outward.  The units are pixels.  The last
%   value must be equal to the number of data pixels.
% p is a vector of ring material property values (one
%   for each ring).  In this case, p is a vector of
%   attenuation values.
%
% OUTPUTS:
% cost is the function evaluation or cost.
%*************************************************************************

function [cost] = cost_002_linatt(n,e,p,Q)

% set up some stuff
P=Q{1};
data=Q{2}(:);
w=Q{3};
```

```
nd=length(data);

% Contstruct a pixelized version of the object (u)
% (convert (n,t,p) into a vector of length nd)

edges=[0;e(:)]/w;
temp=repmat(1:nd,n+1,1)-repmat(edges,1,nd);
x=-diff(min(max(temp,0),1));
uparts=x.*repmat(p(:),1,nd);
u=(sum(uparts))';

% Compute the cost
cost = norm(-P*u/w^2-log(data),2)/sqrt(nd);

return
```

B.7 Objective Function 2 File

```
%*************************************************************************
% cost_004_linatt is a cost functional evaluation for
% use with the mixed-variable optimization X-ray inversion
% project.  It assumes an attenuation reconstruction
% from normalized energy transmission data. The norm assumes
% Guassian additive noise.
%
% This function differs from cost_001_linatt only in the
% last line -- here we use a data fidelity norm on the
% logarithm of the data
%
% USAGE:
% [cost] = cost_004_linatt(n,e,p,Q)
%
% INPUTS:
%   [The inputs constitute an object description]
% Q{1} = P is the Abel projection operator scaled to
%      unit data pixel size
% Q{2} = data is the vector of transmission data values
%      ordered from inside outward.  Values are assumed
%      to be normalized to unity for zero attenuation.
% Q{3} = w is the pixel width (and height) on the
%      detector in real units.
% Q{4} = energy is a vector of intensity normalized
%      energy values describing the source spectrum
% n is the integer number of edges in the object
%   The edge of the data is included as an edge location.
% e is a vector of ring edge locations ordered from
%   inside outward.  The units are pixels.  The last
%   value must be equal to the number of data pixels.
% mu is a matrix of material property values (one row
```

```
%   for each ring).  In this case, p is a matrix of
%   attenuation values such that p(i,j) is the attenuation
%   factor for ring j at the ith energy.
% energy is a vector of energy values corresponding to
%   the attenuation value columns in mu.  The energy is
%   spectrum intensity normalized so that sum(energy)=1.
%
% OUTPUTS:
% cost is the function evaluation or cost.
%*************************************************************************

function [cost] = cost_004_linatt(n,e,mu,energy,Q)

% set up some stuff
P=Q{1};
data=Q{2}(:);
w=Q{3};
nd=length(data);

%%%%% Construct the material ID object %%%%%
e=e/w;
temp=repmat(1:nd,n+1,1)-repmat([0;e(:)],1,nd);
objMID=-diff(min(max(temp,0),1));

%%% Construct attenuation objects for each energy
for j=1:length(energy)
    objMU(j,:)=sum(repmat(mu(:,j),1,nd).*objMID);
end

%%% Calculate the projection
E=zeros(nd,1);
for j=1:length(energy)
   E=E+energy(j)*exp(-(P*objMU(j,:)'/w^2));
end

% Compute the cost
cost = norm(log(E)-log(data),2)/sqrt(nd);

return
```

Bibliography

[1] Aarts, E. and J. K. Lenstra (editors). *Local Search in Combinatorial Optimization*. Princeton University Press, New York, 1991.

[2] Abel, N. H. "Auflosung einer mechanischen Aufgabe". *Math*, 1:153–157, 1826.

[3] Abramson, M. A. "NOMADm optimization software". http://www.afit.edu/en/ENC/Faculty/-MAbramson/NOMADm.html.

[4] Abramson, M. A. *Pattern Search Algorithms for Mixed Variable General Constrained Optimization Problems*. Ph.D. thesis, Department of Computational and Applied Mathematics, Rice University, August 2002.

[5] Abramson, M. A. "Mixed variable optimization of a load-bearing thermal insulation system using a filter pattern search algorithm". *Optimization and Engineering*, 5(2):157–177, 2004.

[6] Abramson, M. A. "Second-Order Behavior of Pattern Search". *SIAM Journal on Optimization*, 16(2):315–330, 2005.

[7] Abramson, M. A. and C. Audet. *Second-order convergence of mesh adaptive direct search*. Technical Report TR05-09, Department of Computational and Applied Mathematics, Rice University, Houston Texas, 2005.

[8] Abramson, M. A., C. Audet, and J. E. Dennis, Jr. "Generalized Pattern Searches with Derivative Information". *Mathematical Programming*, Series B, 100(1):3–25, 2004.

[9] Abramson, M. A., C. Audet, and J. E. Dennis, Jr. *On the convergence of filter pattern search algorithms for mixed variable constrained optimization problems*. Technical Report TR04-09, Department of Computational and Applied Mathematics, Rice University, Houston Texas, 2004.

[10] Abramson, M. A., O. A. Brezhneva, and J.E. Dennis Jr. *Pattern Search in the Presence of Degeneracy*. Technical Report TR03-09, Department of Computational and Applied Mathematics, Rice University, Houston Texas, 2005.

[11] Alberto, P., F. Nogueira, U. Rocha, and L. N. Vicente. "Pattern Search Methods for user-provided points: application to molecular geometry problems". *SIAM Journal on Optimization.*, 14(4):1216–1236, 2004.

[12] Asaki, T. J. *Inverse Abel Transform Regularization*. Technical Report LA–UR–04–4100, Los Alamos National Laboratory, Los Alamos National Laboratory, Los Alamos, New Mexico 87545, 2004.

[13] Asaki, T. J. *Optimization-Based Forward Measurement Operator Tomography*. Technical Report LA–UR–05–2658, Los Alamos National Laboratory, Los Alamos National Laboratory, Los Alamos, New Mexico 87545, 2005.

[14] Asaki, T. J., P. R. Campbell, R. Chartrand, C. Powell, K. R. Vixie, and B. Wohlberg. *Abel Inversion Using Total Variation Regularization: Applications*. Technical Report LA-UR-05-2657, Los Alamos National Laboratory, Los Alamos National Laboratory, Los Alamos, New Mexico 87545, April 2005.

[15] Asaki, T. J., R. Chartrand, K. R. Vixie, and B. Wohlerg. "Abel Iversion using Total-Variation Regularization". *Inverse Problems*, 21:1895–1903, 2005.

[16] Audet, C. and J. E. Dennis, Jr. "Pattern Search Algorithms for Mixed Variable Programming". *SIAM Journal on Optimization*, 11(3):573–594, 2000.

[17] Audet, C. and J. E. Dennis, Jr. "Analysis of Generalized Pattern Searches". *SIAM Journal on Optimization*, 13(3):889–903, 2003.

[18] Audet, C. and J. E. Dennis, Jr. "Mesh Adaptive Direct Search Algorithms for Constrained Optimization". *SIAM Journal on Optimization*, To appear, 2004.

[19] Audet, C. and J. E. Dennis, Jr. "A Pattern Search Filter Method for Nonlinear Programming Without Derivatives". *SIAM Journal on Optimization*, 14(4):980–1010, 2004.

[20] Booker, A. J., J. E. Dennis, Jr., P. D. Frank, D. B. Serafini, V. Torczon, and M. W. Trosset. "A Rigorous Framework for Optimization of Expensive Functions by Surrogates". *Structural Optimization*, 17(1):1–13, February 1999.

[21] Box, G. E. P. "Evolutionary Operation: A Method for Increasing Industrial Productivity". *Applied Statistics*, 6(2):81–101, 1957.

[22] Clarke, F. H. *Optimization and Nonsmooth Analysis*. Wiley, New York, 1983. Reissued in 1990 by SIAM Publications, Philadelphia, as Vol. 5 in the series Classics in Applied Mathematics.

[23] Conn, A. R., N. I. M. Gould, and P. L. Toint. "A Globally Convergent Augmented Lagrangian Algorithm for Optimization With General Constraints and Simple Bounds". *SIAM Journal on Numerical Analysis*, 28(2):545–572, April 1991.

[24] Cremers, C. J. and R. C. Birkebak. "Application of the Abel Integral Equation to Spectrographic Data". *Applied Optics*, 5(6):1057–1063, 1966.

[25] Davis, C. "Theory of Positive Linear Dependence". *American Journal of Mathematics*, 76(4):733–746, 1954.

[26] De Jong, Kenneth A. *An Analysis of the Behavior of a Class of Genetic Adaptive Systems*. Ph.D. thesis, University of Michigan, Ann Arbor, 1975.

[27] Dennis, Jr., J. E. and V. Torczon. "Direct Search Methods on Parallel Machines". *SIAM Journal on Optimization*, 1(4):448–474, 1991.

[28] Dolan, E. D., R. M. Lewis, and V. Torczon. "On the Local Convergence Properties of Pattern Search". *SIAM Journal on Optimization*, 14(4):567–583, 2004.

[29] Fletcher, R. and S. Leyffer. "Nonlinear Programming Without a Penalty Function". *Mathematical Programming*, Series A, 91(2):239–269, 2002.

[30] Glover, F. "Tabu Search–Part I". *ORSA Journal on Computing*, 1(3):190–206, 1989.

[31] Glover, F. "Tabu Search–Part II". *ORSA Journal on Computing*, 2(1):4–32, 1990.

[32] Hilal, M. A. and R. W. Boom. "Optimization of Mechanical Supports for Large Superconductive Magnets". *Advances in Cryogenic Engineering*, 22:224–232, 1977.

[33] Hooke, R. and T. A. Jeeves. "Direct Search Solution of Numerical and Statistical Problems". *Journal of the Association for Computing Machinery*, 8(2):212–229, 1961.

[34] Kak, A. C. and M. Slaney. *Principles of Computerized Tomographic Imaging*. IEEE Press, Inc., New York, 1991.

[35] Karush, W. *Minima of Functions of Several Variables with Inequalities as side conditions*. Master's thesis, Department of Mathematics, University of Chicago, 1939.

[36] Kirkpatrick, S., C. D. Gelatt, and M. P. Vecchi. "Optimization by Simulated Annealing". *Science*, 220(4598):671–680, 1983.

[37] Kokkolaras, M., C. Audet, and J. E. Dennis, Jr. "Mixed variable optimization of the number and composition of heat intercepts in a thermal insulation system". *Optimization and Engineering*, 2(1):5–29, 2001.

[38] Kolda, T. G., R. M. Lewis, and V. Torczon. "Optimization by direct search: new perspectives on some classical and modern methods". *SIAM Review*, 45(3):385–482, 2003.

[39] Kuhn, H. W. and A.W. Tucker. "Nonlinear Programmming". University of California Press, Berkely, CA, 1951.

[40] Lewis, R. M. and V. Torczon. *Rank Ordering and Positive Bases in Pattern Search Algorithms*. Technical Report 96–71, Institute for Computer Applications in Science and Engineering, Mail Stop 132C, NASA Langley Research Center, Hampton, Virginia 23681–2199, 1996.

[41] Lewis, R. M. and V. Torczon. "Pattern Search Algorithms for Bound Constrained Minimization". *SIAM Journal on Optimization*, 9(4):1082–1099, 1999.

[42] Lewis, R. M. and V. Torczon. "Pattern Search Methods for Linearly Constrained Minimization". *SIAM Journal on Optimization*, 10(3):917–941, 2000.

[43] Lewis, R. M. and V. Torczon. "A Globally Convergent Augmented Lagrangian Pattern Search Algorithm for Optimization With General Constraints and Simple Bounds". *SIAM Journal on Optimization*, 12(4):1075–1089, 2002.

[44] Lucidi, S. and V. Piccialli. "A Derivative-Based Algorithm for a Particular Class of Mixed Variable Optimization Problems". *Optimization Methods and Software*, 17(3–4):317–387, 2004.

[45] Lucidi, S., V. Piccialli, and M. Sciandrone. "An Algorithm Model for Mixed Variable Programming". *SIAM Journal on Optimization*, 15(4):1057–1084, 2005.

[46] Maldonado, C. D., A. P. Caron, and H. N. Olsen. "New Method for Obtaining Emission Coefficients from Emitted Intensities: Circularly Symmetric Light Sources". *Journal of Optic Society of America*, 55:1247–1254, 1965.

[47] Nash, S. G. and A. Sofer. *Linear and Nonlinear Programming*. McGraw–Hill, New York, 1996.

[48] Polak, E. and M. Wetter. "Precision Control for Generalized Pattern Search Algorithms with Adaptive Precision Function Evaluations". *SIAM Journal on Optimization*, 16(3):650–669, 2006.

[49] Smith, L. M., D. R. Keefer, and S. I. Sudharsanan. "Abel Inversion using Transform Techniques". *Journal of Quantitative Spectroscopy and Radiation Transfer*, 39:367–373, 1988.

[50] Sriver, T. A., J. W. Chrissis, and M.A. Abramson. "Pattern Search Ranking and Selection Algorithms for Mixed Variable Stochastic Optimization". 2004. Preprint.

[51] Torczon, V. "On the Convergence of Pattern Search Algorithms". *SIAM Journal on Optimization*, 7(1):1–25, February 1997.

Vita

Second Lieutenant Kevin R. O'Reilly graduated from East Brunswick High School in East Brunswick, New Jersey. He entered undergraduate studies at the United States Air Force Academy in Colorado Springs, Colorado where he graduated with a Bachelor of Science degree in Space Operations in June 2004 and was recognized as a Distinguished Graduate. Following graduation he was commissioned an officer in the United States Air Force and was assigned to Wright-Patterson AFB where he entered the Graduate School of Engineering and Management, Air Force Institute of Technology to pursue a Masters of Science degree in Space Systems. Upon graduation, he will be assigned to Vandenberg AFB, California where he will receive technical training in the Space and Missile career field in order to become a space and missile operator.

REPORT DOCUMENTATION PAGE

Form Approved
OMB No. 074-0188

The public reporting burden for this collection of information is estimated to average 1 hour per response, including the time for reviewing instructions, searching existing data sources, gathering and maintaining the data needed, and completing and reviewing the collection of information. Send comments regarding this burden estimate or any other aspect of the collection of information, including suggestions for reducing this burden to Department of Defense, Washington Headquarters Services, Directorate for Information Operations and Reports (0704-0188), 1215 Jefferson Davis Highway, Suite 1204, Arlington, VA 22202-4302. Respondents should be aware that notwithstanding any other provision of law, no person shall be subject to an penalty for failing to comply with a collection of information if it does not display a currently valid OMB control number.
PLEASE DO NOT RETURN YOUR FORM TO THE ABOVE ADDRESS.

1. REPORT DATE *(DD-MM-YYYY)*	2. REPORT TYPE	3. DATES COVERED *(From – To)*
23-03-2006	**Master's Thesis**	24-08-2004 – 23-03-2006

4. TITLE AND SUBTITLE

Quantitative Object Reconstruction using Abel Transform Tomography and Mixed Variable Optimization

5a. CONTRACT NUMBER

5b. GRANT NUMBER

5c. PROGRAM ELEMENT NUMBER

6. AUTHOR(S)

O'Reilly, Kevin, R., Second Lieutenant, USAF

5d. PROJECT NUMBER
2005-159

5e. TASK NUMBER

5f. WORK UNIT NUMBER

7. PERFORMING ORGANIZATION NAMES(S) AND ADDRESS(S)
Air Force Institute of Technology
Graduate School of Engineering and Management (AFIT/EN)
2950 Hobson Way
WPAFB OH 45433-7765

8. PERFORMING ORGANIZATION REPORT NUMBER

AFIT/GSS/ENC/06-1

9. SPONSORING/MONITORING AGENCY NAME(S) AND ADDRESS(ES)
Los Alamos National Laboratory
Attn: Dr. Thomas J. Asaki
CCS-2, Mail Stop D413
Los Alamos NM 87545 Comm: (505)-667-5787

10. SPONSOR/MONITOR'S ACRONYM(S)
LANL

11. SPONSOR/MONITOR'S REPORT NUMBER(S)

12. DISTRIBUTION/AVAILABILITY STATEMENT
APPROVED FOR PUBLIC RELEASE; DISTRIBUTION UNLIMITED.

13. SUPPLEMENTARY NOTES

14. ABSTRACT

Researchers at the Los Alamos National Laboratory (LANL) are interested in quantitatively reconstructing an object using Abel transform x-ray tomography. Specifically, they obtain a radiograph by x-raying an object and attempt to quantitatively determine the number and types of materials and the thickness of each material layer. Their current methodologies either fail to provide a quantitative description of the object or are generally too slow to be useful in practice. As an alternative, the problem is model here as a mixed variable programming (MVP) problem, in which some variables are nonnumeric and for which no derivative information is available. The generalized pattern search (GPS) algorithm for linearly constrained MVP problems is applied to the x-ray tomography problem, by means of the NOMADm MATLAB® software package. Numerical results are provided for several test configurations of cylindrically symmetrical objects and show that, while there are difficulties to be overcome by researchers at LANL, this method is promising for solving x-ray tomography object reconstruction problems in practice.

15. SUBJECT TERMS
X-ray Tomography, Abel Transform, Mixed Variable Programming, Pattern Search Algorithms, Constrained Optimization, Quantitative Object Reconstruction

16. SECURITY CLASSIFICATION OF:			17. LIMITATION OF ABSTRACT	18. NUMBER OF PAGES	19a. NAME OF RESPONSIBLE PERSON
REPORT	ABSTRACT	c. THIS PAGE			LtCol Mark A. Abramson
U	U	U	UU	97	19b. TELEPHONE NUMBER *(Include area code)* (937) 255-3636, ext 4524;mark.abramson@afit.edu

Standard Form 298 (Rev: 8-98)
Prescribed by ANSI Std. Z39-18